ABSTRACT

KOMMAJOSHYULA, PRADYUMN. Experimental Study of Nano Electro Machining. (Under the direction Dr. Paul Cohen.)

Scanning Probe Lithography (SPL) is one of the methods used for synthesizing nano-structured materials and devices. SPL potentially 3D, relatively fast and needs no expensive masks. Nano milling and nano electro machining are recent developments in SPL. Nano electro machining is analogous to electric discharge machining which removes material by discharge between two electrodes (work piece and tool). The nano-scale version involves Atomic Force Microscope (AFM) tip and sample act as electrodes. Previous works removed material by adding negative pulses to AFM tip. These attempts resulted in hole with diameters typically spanning around 100 nm in width or diameter and 50 nm in depth. Some environments in which nano electro machining was done include air and dielectric oil. Some sample materials include Highly Ordered pyrolitic Graphite (HOPG), gold, copper. Here an experimental study of the process parameters of the nano electro machining is done using HOPG. The process parameters peak to peak voltage of the pulse and number of pulses or time of machining are studied using factorial experiments by fabricating holes with several combinations of these parameters. Out of these two parameters peak to peak voltage or simply voltage was found have a much greater impact on the material removed on the HOPG work-piece. Further fabrication of trenches or slots was also found to be feasible. In addition nano electro machining HOPG using a polycrystalline silver nanowire attached to the AFM tip was also found to be feasible.

Finally the dimensions of holes made by the nanowire and standard tip were compared and their differences was briefly discussed using a rough model.

Experimental Study of Nano Electro Machining

by
Pradyumn Kommajoshyula

A thesis submitted to the Graduate Faculty of
North Carolina State University
in partial fulfillment of the
requirements for the Degree of
Master of Science

Industrial Engineering

Raleigh, North Carolina

2013

APPROVED BY:

_______________________ _____________________
Dr. Ronald Scattergood Dr. Jingyan Dong

____
Dr. Paul Cohen
Chair of Advisory Committee

BIOGRAPHY

Pradyumn Kommajoshyula was born in Chennai, India on April 30th 1989. He completed the greater part of his school education there and finished high school in Boston School, Chennai, India. In 2006, he began college at Velammal Engineering College, under the umbrella of Anna University, majoring in Mechanical Engineering. He enrolled for the Master of Science program in 2010 at North Carolina State University, Raleigh, NC, USA after completing his bachelor's degree in the same year.

ACKNOWLEDGMENTS

I would first like to thank my advisors, Dr. Paul Cohen and Dr. Jingyan Dong for all of their guidance and support, during the research. I also want to thank Dr. Ron Scattergood for being a committee member, as well as for his guidance. I am indebted to Li Zhang for all his assistance without which this would not have been possible. I also thank all the other students in Dr. Cohen and Dr. Dong's group for their assistance. Finally, I would like to thank my family and friends for their support throughout my graduate studies.

TABLE OF CONTENTS

LIST OF TABLES

LIST OF FIGURES

1. INTRODUCTION

Increasing demands of the electronics sector is pushing the semiconductor industry into reducing the size of transistors, photodiodes, emitters and sensors from micro-scale to nano-scale. The advantage of nano-scale features is not just the obvious size advantage but also exploiting quantum effects [1]. Fabrication of devices in the nano-scale involves several choices of processes like etching [2] and deposition [3] which is top-down and bottom-up respectively. However there are several devices that need to be selectively etched or deposited in order to fabricate them. Most of these involve slots trenches or holes. The fundamental limit of photo-lithography is light itself. The resolution of the nano-scale features are limited by the wavelength of light. Thus these smaller patterns are made by other means with scanning probe lithography being one of them. Electron beam lithography [4] which can easily fabricate these features places many constraints on the equipment used because of the requirement of vacuum. Scanning probe lithography facilitates relatively simple handling of equipment. There are many forms of scanning probe techniques some are the oxidation and mechanical scratching using an atomic force microscope. The other is the scanning tunneling microscope lithography. A relatively new type of lithography is the spark erosion, “electric pen” or the nano electro machining. This has several advantages over the other processes which are briefly discussed in the next section. Potential applications include plasmonic LEDs [5] and the quantum anti-dot arrays [6]. One of the patterned substrate fabricated in this work using this process lithographically resembles a quantum anti-dot array. In this thesis the process parametrical dependence of dimensions of these features are explored.

2. LITERATURE REVIEW

2.1 Scanning Probe Lithography

The atomic force microscope was primarily built for imaging surfaces of materials [7] or for imaging the nano-scale patterns fabricated on the material [8]. The AFM can be used to measure electrical properties [9], magnetic properties [10] or measuring surface topology [11]. However, the atomic force microscope has also been used to fabricate nano-scale patterns. Most of these involve the tip removing material [12] [13] [14] and others build up or change the composition of the material [15] [16]. Usually this method of fabrication produces patterns in the form of holes or trenches [17]. In many cases this is not the final product or device and further processing is needed. In case of mechanical scratching the photo-resist needs to be removed after etching the material underneath.

2.2. Mechanical Scratching and Nano-milling

In this form of lithography the tip approaches the surface, indents it and is moved to form a pattern. The tip can be move to plough the material to make nano-scale slots [18]. However due to the nature of the process it is almost always limited to soft materials although there were exceptional cases [19]. This leads to making patterns only on soft polymers like photo-resists deposited on a substrate material and then further processed to make the desired device [20]. Using this method the AFM tip is used to make nano-scale trenches on the photo-resist which is deposited on the substrate thus exposing the substrate underneath for etching patterns. The patterns can be used as a part of a device such as a micro or nano-sensor or an actuator [21]. There are several improvements to this process to remove more material including vibrating the sample on a custom made z-stage [22]. A hardened diamond-like carbon tip can remove a large volume of material by vibrating the stage x and y direction and may be even in the z direction [22]. This simulates the milling machining operation in machine shop.

2.3. Oxidation and Scanning Tunneling Lithography

Another lithography process involves patterning by means of electrical contact. The tip is approached to the surface and instead of mechanically ploughing or scratching; an electric field is applied between the tip and surface. This electric field causes some manipulation on the surface. The surface features formed are in most cases oxides of the work-piece material. The electric field can be direct current or a pulse. This electric field induced oxidation [23] can be used for further processing, making the desired devices. The areas where the AFM tip enabled oxidation produce a different reaction to etching agents [25]. This can be used to make patterns as the etching material removes material around the oxidized regions. The second kind of manipulation is scanning tunneling lithography. Scanning tunneling microscopy is used to map the surface topology of a material by measuring the tunneling current between the tip and the sample while scanning [25]. The STM can also be used for patterning as a chemical reaction by the free charges of the tunneling current can be used to remove or etch the material [26, 27].

2.4 Nano Electro Machining

A new kind of lithography performed by means of applying basically an electrical pulse to sample via the AFM tip is the nano electro machining. Nano electro machining is analogous to the electric discharge machining at the macro scale. Electric discharge machining or spark erosion is a non-traditional machining process at the macro scale. This involves material removal by means of spark erosion between the tip which acts as the electrode and the conducting sample in presence of a dielectric medium. This process has also been replicated in the micro-scale [28 to 30] in which pulses (hundreds of microseconds in periods) are applied between a tool (ex: Tungsten and 50 um diameter) and a conducting work piece in presence of a hydrocarbon based dielectric. The electric discharge between the tool and work-piece creates in holes of around 100 um in diameter. The material is eroded by the thermal energy that results from the discharge [29].

The nano-scale version is performed by treating AFM tip (as opposed to the micro fabricated and cylindrical tool in micro EDM) and sample surface as electrodes and applying a pulse in between. The tip is given the negative pulse and the sample which is grounded and gets eroded. The mechanism of material removal in the nano electro machining is not known although; a previous publication ruled out some of the possible mechanisms such as electro-migration [31]. This process has some advantages over the processes previously mentioned. As this is direct fabrication, further process is not needed. It can be only performed on conducting materials. However the patterns are directly fabricated on the substrate and there is no need for further processing like etching or removal of photo-resist etc. Most of the experiments done here required no special modifications of the AFM system other than the coating of the cantilever (40 to 60 nm of gold and palladium by sputtering) only to make it conductive.

As the mechanism is still not completely clear, here the dependence on several parameters of the width of the geometries and dimensions of eroded areas are explored by means of design of statistical experiments. Many of the previous works were performed with the medium between the tool and the work-piece being dielectric oil [32, 33]. Also these were performed on a system designed for scanning tunneling microscopy and hence the precise measurement of distance between the tip and substrate was possible. This facilitated the measurement of I-V characteristics and Paschen curves which provided a deeper understanding of the nano electro machining process. In one experiment, a tungsten electrode was used on a gold sample showed formation of tungsten carbide and oxide precipitates in a nano-crystalline form. This carbide formation enhanced the nano electro machining capability. It was hypothesized that the mechanism was because of the dielectric breakdown with some contribution of tunneling electrons. The tool after nano electro machining had a smaller radius than the original electric field assisted nucleation of nano-crystalline tungsten oxide and carbide phases on tool surface and sub-surface was observed. In another study the tip was coated with Ir-Pt and performed on <111> gold under dielectric oil. The material removal rate was 141 cu. nm/second. The authors have demonstrated nanometer scale material removal as small as 10 nm in diameter and under 1 nm in depth. Another study was done on highly ordered pyrolytic graphite (HOPG) without dielectric medium and a coated tip [34]. This was done with carbon nanotube tip as well as standard tip. The equipment used there was a scanning tunneling microscope and had feature to precisely measure tip-surface distances and I-V characteristics. It was hypothesized that the possible removal mechanism was that tunneling electrons induced chemical reaction. The I-V characteristics showed that the nano electro machining mechanism was influenced the maximum by voltage and not current. In this study, a comparison between voltage and time of machining was thoroughly investigated. Due to equipment restrictions it was not possible to measure the I-V characteristics nor accurately estimate the tip-sample distance.

3. EXPERIMENTS

3.1 Equipment and Setup

The experiments were conducted using a Park Systems XE-70 Atomic Force Microscope. This is a standard AFM which scans images by the XYZ scanner and a micro-cantilever. It is placed on a Minus K vibration stabilizer and enclosed in an acoustic chamber. The AFM tips used for this experiment are the following:

1. Park Systems NCHR (stiffness: 40 N/m , radius: <30 nm, mode: non-contact)
2. Nanoandmore Tap300 (stiffness: 40 N/m , radius: <30 nm, mode: non-contact)
3. Ktek Tetra-16(Au) 40 N/m (stiffness: 40 N/m , radius: 50 nm, mode: non-contact)

For all the experiments the first two tips were coated with approximately a total thickness of 40 nm to 60 nm of gold and palladium by sputtering to make them conductive. The equipment for pre-coating SEM samples, at NCSU analytical instruments facilities (JEOL 6400F), was used to coat these tips. The coating increases the tip radius, so the actual tip radius is higher than the one specified above and depends on the coating thickness. The third tip was already coated with gold and titanium (total thickness of 40 nm) by the manufacturer.

One of the samples used was aluminum film. This sample was prepared by thermally depositing aluminum on silicon <100> wafers with a thickness of about 100 nm. The other was a 10 x 10 x 3 mm highly ordered pyrolithic graphite (HOPG). The samples were mounted on the standard stage provided by the AFM system. The sample, after testing for conductivity, is then grounded using a wire attached to the AFM ground. Two electrical sources were used. One was a Keithley source meter was used for DC source while the Agilent signal generator was used for pulsed signals. The 'signal access module' provided by Park Systems was a box with BNC ports connecting to various systems of the AFM including tip bias, sample bias, various imaging signal I/O etc. This access module can be used to send custom signals into the AFM for various purposes. In this setup we send the custom electric pulse into the AFM via the access module. The BNC from the Agilent or the Keithley source meter is directly connected to the 'tip bias' port of the signal access module. This setup ensures that the signal from the signal generator directly goes to the AFM cantilever. Figure 1 shows a schematic of the setup.

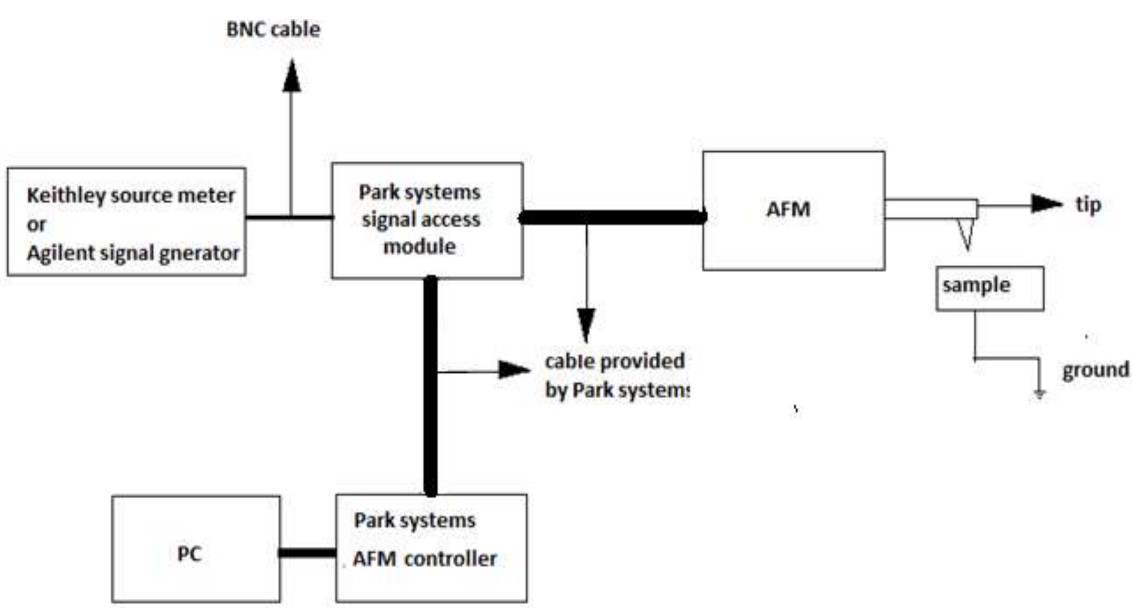

Figure 1 Schematic experimental setup of the system.

All of the entities in Figure 1 except ‘Keithley source meter..’ and the ‘ground’ are provided by Park Systems and from the normal setup. Connecting a BNC from the Agilent to the ‘tip bias’ port of the signal access module sends the signal directly to the tip. Any wire attached securely to the sample and the ground forms the only addition to the normal setup of AFM in order to perform this experiment.

In addition to these two connections a conductive epoxy can be added to the ‘chip carrier’ plate which contains the AFM cantilever which attached to the z-stage. This ensures that the cantilever receives the signal as illustrated in Figure 2. The chip carrier plate is attached to the z-stage and holds the chip and cantilever and it is shown in the Figure 2. The chip carrier plate is attached to the z-stage and holds the chip and cantilever with, conductive epoxy. All of the experiments except in case of aluminum used the Agilent signal generator. To perform nano electro machining in case of HOPG sample the tip must be approached to the sample and held stationary. XEL is a software package provided by Park Systems which is used for performing lithography using the AFM. XEL provided by Park Systems can be used to place the tip exactly at the spot desired and a pulse can be sent to it. The Agilent signal generator allows the user to control the number of pulses, peak-to-peak voltage, frequency etc. In case of HOPG sample the pulse, nature and details are given in Table I. Peak-to peak voltage or simply voltage and the number of pulses or simply pulses can vary in an experiment.

Figure 2 Conductive epoxy to the chip carrier plate.

The aluminum sample was used only to check whether the AFM system with the current setup is capable of performing lithography using this process before using the HOPG sample. Details of aluminum sample and the experiment made using it are given in Appendix D.

3.2 Outline of the Experiments

. The aim of the experiments is to determine the dependence of dimensions of the resulting holes on the input parameters. As observed in Table I many parameters can be altered. In this work only two parameters were altered: the peak-to-peak voltage and the number of pulses. From this point on the term voltage will refer to the peak-to-peak voltage as a short hand notation. The other parameters such as duty cycle, frequency etc., are held constant throughout this work, unless otherwise explicitly stated.

The first experiment was exploratory in nature. The experiment consists of a wide range of voltages and a limited range of pulses. The next two experiments were performed to quantify the process repeatability. One of these is to find the threshold of voltage for which nano electro machining becomes repeatable. The other one was to quantify the repeatability over a large range of number of pulses.

Table I The parameters used in all experiments on HOPG

<table>
<tr><td colspan="4">Constant parameters</td><td colspan="2">Variable parameters</td></tr>
<tr><td>To be set using the AFM system</td><td colspan="3">To be set using Agilent signal generator</td><td colspan="2">To be set using Agilent signal generator</td></tr>
<tr><td>Set point</td><td>Frequency or period</td><td>Duty cycle</td><td>offset</td><td>Peak to peak voltage</td><td>Number of pulses</td></tr>
<tr><td>5 nN</td><td>20 Hz or 50 ms</td><td>50 %</td><td>Negative 60% of peak to peak voltage</td><td>Varies</td><td>varies</td></tr>
</table>

To examine the dependence of dimensions of the resulting hole on the input parameters, an nxn (for some integer n) factorial experiment was performed with voltage and number of pulses as the factors. The method is to make a single hole by applying a number of pulses with some voltage and then fabricate more holes each with an increased voltage (all with the same number of pulses). The next iteration would be to fabricate the same number of holes with the same incremental voltage, but each of them with an increased number of pulses than the previous iteration. More iterations can be performed each with increased number of pulses. The order in which the iterations were performed may differ with each experiment. For example, an nxn matrix of holes on the HOPG sample corresponds to an nxn factorial experiment with voltage and the number of pulses.

Thus the aim of the three experiments mentioned above can be summarized as follows:

1. Exploring all the range of voltages and small range of pulses
2. Exploring threshold voltage at which the process becomes consistent
3. Quantifying repeatability over a larger range of pulses

In addition to the experiments described above two additional experiments were performed. One of these is to fabricate a feature on the sample other than a hole; a trench. The other experiment is a factorial experiment similar to the one described above, with the only difference being that the aspect ratio of the AFM tip is much lower.

The experimental procedure for these experiments is described below.

The sample used here is 10x10x3 mm highly ordered pyrolitic graphite. The sample is hence chosen because of its high atomic flatness. As explained in the previous Section, the sample is placed on the standard sample holder and a wire connects it to the ground. In a typical experiment the tip is approached to the sample surface and it is held stationary and given a voltage. The tips used were old tips which were used for some mechanical scratching experiments. Each tip was coated with palladium and gold of around 40 to 60 nm total thickness.

In addition to the above experiment, a separate study was conducted, the purpose of which was to test the feasibility of performing nano electro machining by attaching a nanowire to a standard AFM tip. The nanowire (made of polycrystalline silver) is attached by a standard AFM tip by means of an epoxy. The nanowire is estimated to have a diameter of around 100 to 150 nm and a length of about 2 to 3 um. Since the nanowire is attached to the AFM tip by means of a non-conducting epoxy, the AFM tip along with the nanowire is coated with gold and palladium with a combined thickness of 40 to 60 nm in the same manner mentioned in the beginning of Section 3.1. The tip with the nanowire is mounted on the AFM and the procedure used for nano electro machining is the same as the one described in Section 3.1.

4. RESULTS AND DISCUSSION

When material was removed by nano electro machining the pattern left on the substrate resembles a cone, similar to the cross Section of the AFM tip. Therefore the features have two measureable parameters, height and diameter of the cone which are the diameter and height of the cone. In case of trenches or series of holes the pattern formed was in the form a V-shaped groove and the results were characterized in terms of width and depth of the groove. The following Sections show the variations of the dimensions of the features using factorial experiments for the three scenarios: holes using a standard tip, trenches or slots or series of holes using standard tip and stray holes using a nanowire tip.

4.1 Study of the Resulting Hole Dimensions made by a Wide Range of Voltages

The aim of the following experiment was to examine the dimensions of the resulting hole and how they depend on a large range of voltage and relatively small size of the holes. To examine the dependence of dimensions of the resulting hole an 12x3 factorial experiment was performed with voltage and number of pulses as the factors. Experimentally, this 12x3 factorial experiment translates into a matrix of holes with three rows and twelve columns on the HOPG surface. Each row contains twelve holes each made with a different voltage and constant number of pulses. The voltage is in a decreasing order from 9.5 V to 4 V with 0.5V as an interval. Each column contains holes made by an increasing number of pulses 1, 4 and 8. The last column was given a voltage of 7 V and with 1, 4 and 8 pulses to demonstrate that the decreasing hole size was not due to wearing of the tip or some chronological phenomenon. Table II shows the parameters used throughout this experiment.

Table II Parameters used in experiments with the standard tip

Constant parameters				Variable parameters	
To be set by using the AFM control	To be set using Agilent signal generator			To be set by using Agilent signal generator	
Set point	Frequency or period	Duty cycle	offset	Peak-to peak voltage	Number of pulses
5 nN	20 Hz or 50 ms	50 %	Negative 60% of peak to peak voltage	4 V to 9.5 V	1,2,4,8,12

4.1.1. Variation of the Resulting Hole Dimensions made by a Wide Range of Voltages

When the AFM tip is placed above the substrate and given a pulse of sufficient voltage, material was removed and a hole was formed. The dimension of the hole, resembling a cone, showed a dependence on the voltage and the number of pulses. A non-contact mode image of the sample after the experiment measured the dimensions (depth and diameter) of the holes formed. Figure 4(a) and (b) graph depth as a function of voltage and pulses. It is clear that the width (diameter) and depth decrease with decreasing voltage and also increase with increasing pulses. Additional results can be found in the Appendix A. The threshold of nano electro machining is found to be 4 V as there is no material removal when the voltage is lower. Also the last 3 holes in Figure 3 (a) were made by 7 V and were made after fabricating the 33 holes made from 9.5 V to 4 V.

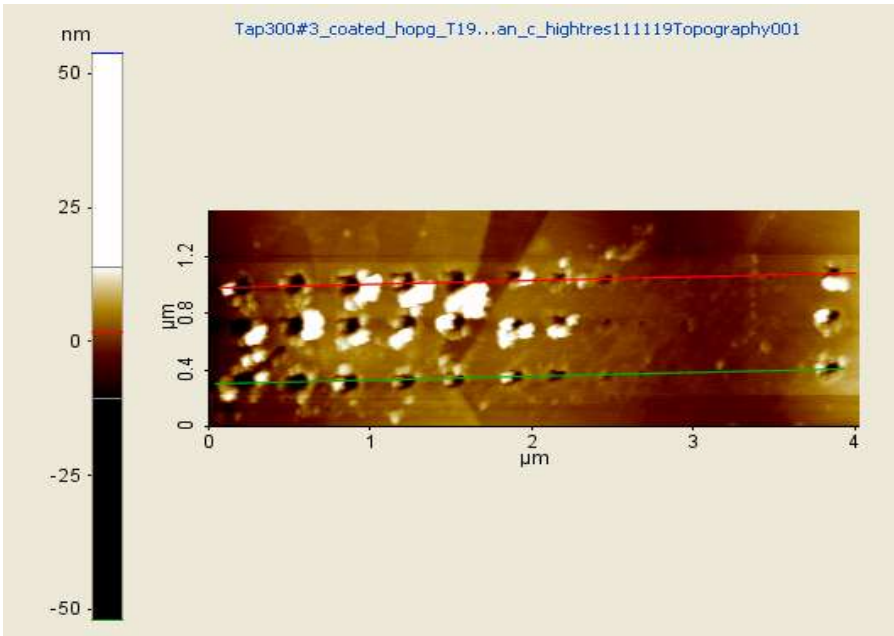

(a)

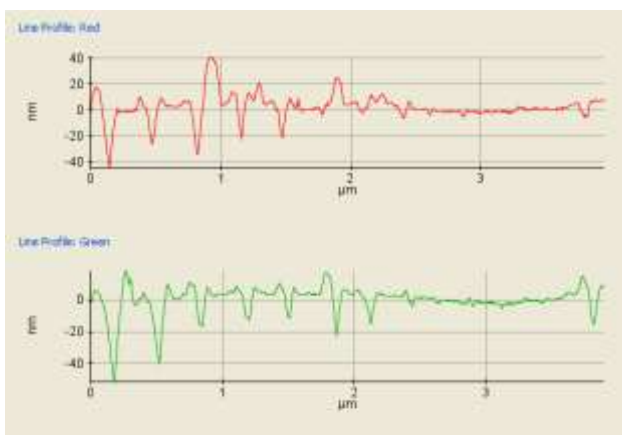

(b)

Figure 3 (a) AFM image of a 12x3 factorial experiment done with 9.5 V to 4 V (from left to right) in steps of 0.5 V and 1,2,4 (top, middle and bottom row in that order) taken in non-contact mode (b) is the profilometer image.

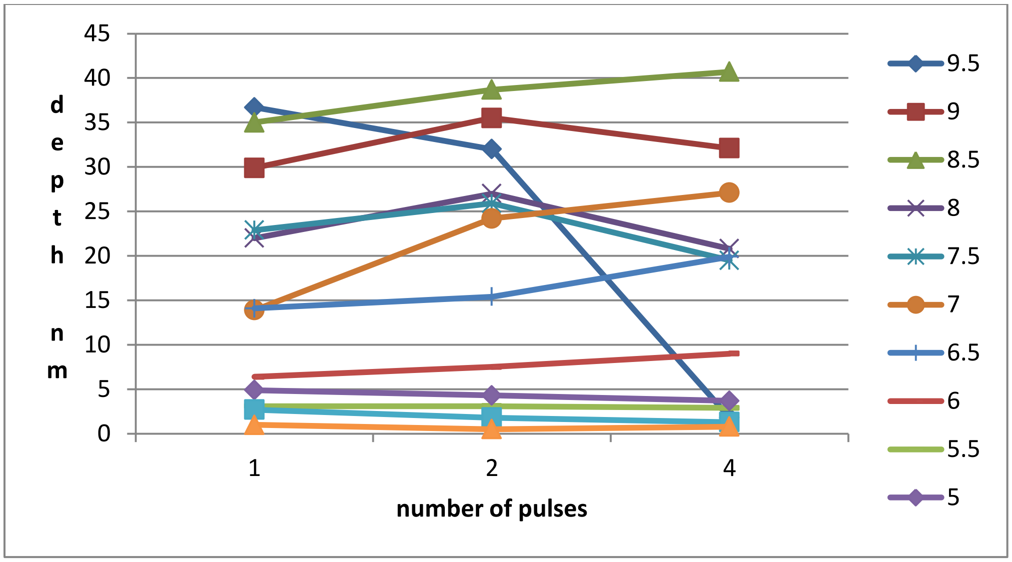

(a)

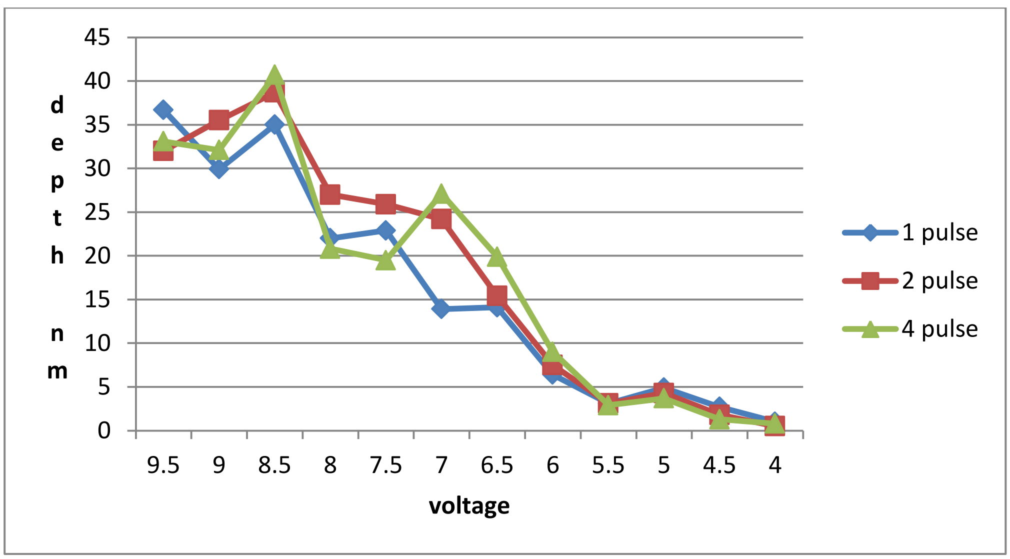

(b)

Figure 4 (a) Plots of depth vs. number of pulses for each voltage and (b) depth vs. voltage for each pulse.

This illustrates that the decrease in hole size is not a chronological phenomenon such as tip wear and the hole diameter and depth depend strongly on voltage.

The number of pulses, however, seemingly has relatively less influence on the dimensions of the holes. This may be because the melting of the tip material may have resulted in debris that is deposited on the sample. This is investigated more thoroughly in the next experiment in subsequent Sections. By this, one can concur that nano electro machining occurs at a wide range of voltages from 9.5 V to 4 V (and beyond) and 4V is the threshold of nano electro machining. The hole diameter and depth strongly depends on the voltage. The next step is to quantify the dependence of voltage and number of pulses and the repeatability.

4.2 Study of Repeatability

It was established by the previous experiment that the threshold voltage for nano electro machining is 4 V. However, it is found that the process is not very repeatable for low voltages. Attempts to make holes with 4 V to 5 V had a low success rate i,e no material removal was observed in many attempts. In this regard, there was a need to establish a 'threshold' for the minimum voltage that produced some feature on the sample every time.

The aim of the following experiment was to characterize the repeatability of the process. To determine the repeatability threshold voltage the following experiment was performed. The range of voltage in the experiment was small: 7 V, 6 V and 5 V. The number of pulses in the experiment were 1, 4 and 8. The experiment was a 3x3 factorial experiment was performed similar to the one described in the previous Section. But here, it is needed to determine the threshold voltage for repeatability; hence this factorial experiment was repeated four times. The aim is to determine the voltage the process begins to be replicable.

4.2.1 Characterization of Repeatability

The factorial experiment performed with a small range of voltage ranging 7 V, 6 V and 5 V and 1, 4 and 8 pulses revealed the repeatability threshold as 5 V. All holes made by 5 V produced some features. The factorial experiment is a 3x3 experiment with each hole made by a different voltage: 7V, 6 V, 5 V and number of pulses: 1, 4, 8. This experiment was performed four times to investigate repeatability and also to explore the minimum voltage threshold at which it is possible to repeat the experiment. This experiment also reveals that at voltages around 5 V the size of the hole depends on the state of the tip prior to nano electro machining. Figure 5 below shows AFM image of the 3x3 arrays. It can be noted that the order in which they were fabricated differs. Out of the four experiments, two were done left to right (7V, 6 V,5 V in that order) and the other two were done right to left (5 V, 6 V ,7 V in that order). Illustrative details of this can be found in the Appendix C. The very first of these four was left to right and the next two were right to left and last one was again left to right (explained pictorially in Appendix C). It can be seen from the final AFM image in Figure 5 and also those in Appendix B that there is some difference in dimensions of the ones fabricated with 6 and 5 V depending on the order in which they were done. When it was done from left to right (7 V, 6 V, 5 V in that order) the holes (made from 6 V and 5 V) were significantly larger those made by right to left (5V, 6V, 7 V in that order). The fourth and last trial was left to right and the holes made were much bigger than those of the previous two trials which were right to left. This suggests that the wear of the tip is not the cause. Two hypotheses suggest that heat from high voltage machining (7 V) either heated the tip and produced thermionic electrons that helped remove material or heated the sample and lowered the energy needed to remove material per unit volume.

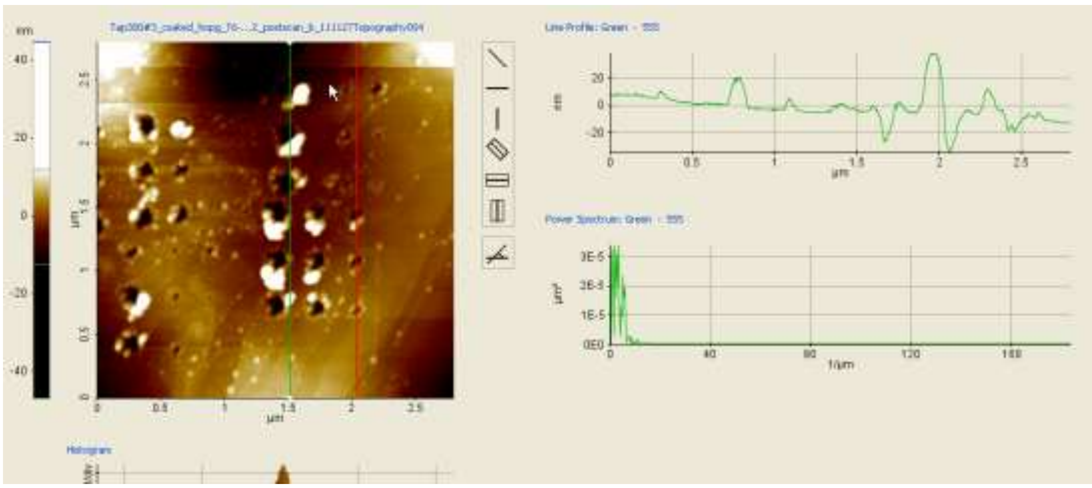

Figure 5 AFM image of four 3x3 arrays on the left hand side. Each array consists of 9 holes made in a factorial experiment with 7 V, 6 V and 5 V (in that order) and 1,4 and 8 pulses. The green line indicates the cross-Section of some of the holes that is found in the right hand side of the figure.

It can be concluded that when doing an experiment with this process using multiple voltages, it is most expedient to start with the highest voltage if one wants the holes to be as large as possible. Figure 6 shows the plots of average depth against the voltage and the pulses. More plots of width, depth and computed volume of individual holes can be found in the Appendix A. This reveals that the voltage has a stronger influence than the number of pulses on the dimensions of the holes. This influence is more thoroughly investigated in an experiment with a relatively large range of pulses in the subsequent Section.

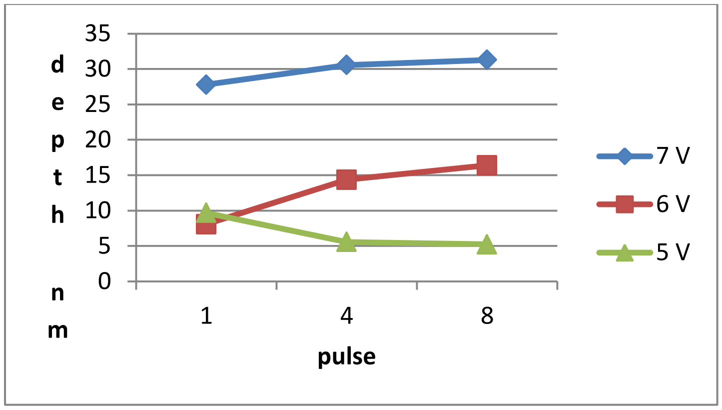

(a)

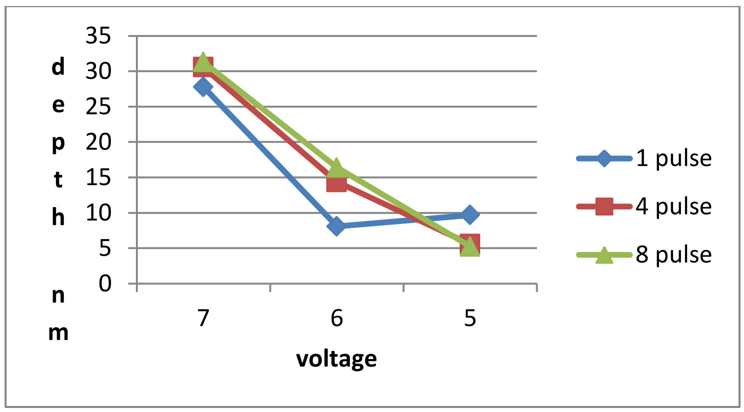

(b)

Figure 6 (a) Plots of average depth vs. number of pulses for each voltage and (b) average depth vs. voltage for each pulse.

4.3 Investigation of Voltage and Pulses on the Dimensions

The threshold for repaetability was established by the previous experiment and the repeatability was quanitfied for a large range of number of pulses, namely 4, 8 and 12. The objective of this experiment is to quantify the repeatability over a large range of pulses that might, therefore, determine the repeatbility of the process. The experiment is a 3x3 factorial experiment with 7 V, 6 V and 5 V and the number of pulses were 4, 8 and 12. This 3x3 experiment was repeated four times. All the parameters are the same as in the experiment described in 3.3 except for the peak-to-peak voltage and number of pulses.

4.3.1 Influence of Voltage and Pulses on the Dimensions and Repeatability

This experiment serves to quantify the repeatability over a larger range of pulses now that the threshold of voltage for repeatability is established by the previous experiment as 5 V. Figure 7 shows the AFM image of one of the 3x3 experiment which was done. The other three aren't shown to eliminate redundancy. The hole apparently replicated the shape of the tip. The odd shape of the tip may be because of its function as mechanical plough tool prior to the use in this experiment.

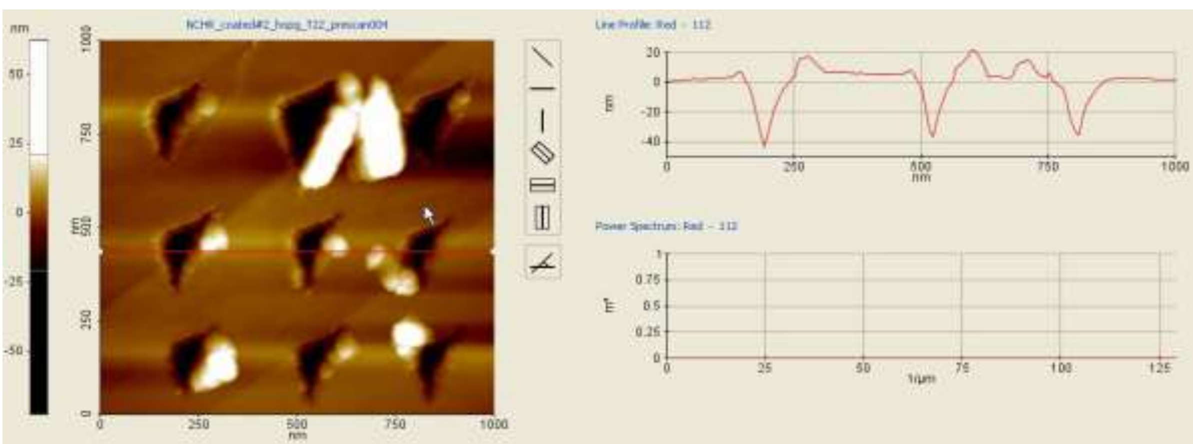

Figure 7 Left hand side is the AFM image of a 3x3 array made in factorial experiment. The input number of pulses increase in steps of 4,8 and12 with each hole from left to right. The input voltage increases in steps of 7 V, 6 V and 5 V in that order, with each hole from top to bottom. Right hand side depicts the cross Section of some of the holes corresponding to the red line on the L.H.S.

Figure 8 shows the average depth as a function of voltage and pulses. The average depth is average of the four trials. Also out of the total 36 holes fabricated in this experiment one did not form properly (highly diminished possibly due to large amount of impurities on the surface) and it was excluded from the result. More plots can be found in the Appendix A. To quantify the repeatability a linear statistical model is proposed. The data for this analysis is from the 3x3 factorial experiment using the standard tip. ANOVA is performed using Excel and Minitab (not shown in the document). The preliminary model is Y = P + V. 'Y' to the width (diameter) of the holes formed and V refers to the peak to peak voltage of the pulse and P is the number of pulses. The p-value of V is in the order of 1 x 10^-7 and that of P is around 0.71. This illustrates that the voltage has a much stronger influence than the number of pulses on the diameter of the holes. (The results were similar for both depth and width (diameter) of the holes).

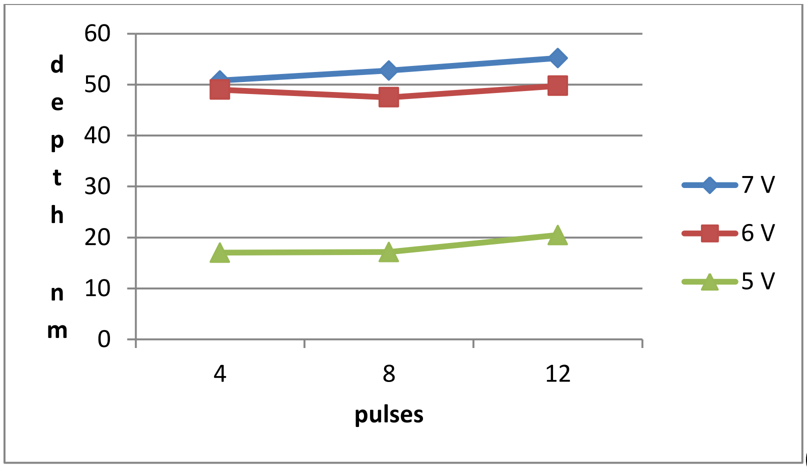

(a)

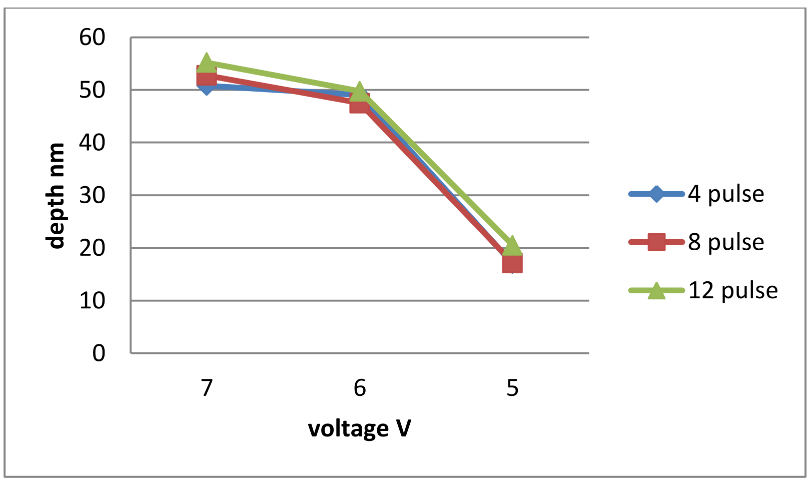

(b)

Figure 8 (a) Plots of average depth vs. Number of pulses for each voltage and (b)plot of average depth vs. voltage for each pulse.

The R squared was just under 0.50 which means there is a huge variation in width (diameter) of the holes. Several other models were tried to obtain a larger R squared. The model that yielded the highest R squared (0.65) was the following model: Y = ln(PV) + ln(P) (Y is the width(diameter) of holes). The Table III (shown below) is the ANOVA result corresponding to the experiment with 7 V, 6 V, 5 V and 4, 8, 12 pulses for the hole diameter with this model (Y = ln(PV) + ln(P)). From Table III, the variables 'X variable 1' corresponds to ln(PV) and 'X variable 2' corresponds to ln(P). The model described above gave the highest R squared. Thus the dimension of the width (diameter) of the hole is best modeled by ln(PV) + ln(P). The p-values of both variables (ln(PV) and ln(P)) are in the order of 1 x 10^-8 or less, meaning that ln(PV) and ln(P) terms are highly significant in predicting the width (diameter) of the holes. The overall interpretation of the result is as follows:

- The width (diameter) is best modeled as a function as logarithm of Voltage and number of pulses (Y = ln(PV) + ln(P)).
- Voltage has a stronger influence on the width (diameter) than the number of pulses.
- The experiment only somewhat repeatable with a large variation in hole dimensions (R squared is 0.65), perhaps due to impurities, temperature, humidity or uneven surface.
- Very similar results were obtained in case depth of the holes (see Appendix A).

The number of pulses is proportional to the duration of machining. If this time duration can be thought of as a quantity related to current or the charge per unit time then by the result above voltage is much more important for material removal than the current.

Table III ANOVA of the 3x3 factorial experiment with 7V,6V and 5 V and 4,8,12 pulses

3x3 experiment

Variables: **Voltage 'V'** {5,6,7 V}; number of **pulses 'P'** {4,8,12}

Output: **Width Y**

Model: **Y = ln(PV) + ln(P)**

SUMMARY OUTPUT

Regression Statistics	
Multiple R	0.811195549
R Square	0.658038218
Adjusted R Square	0.636665607
Standard Error	23.53757253
Observations	35

ANOVA

	df	*SS*	*MS*	*F*	*Significance F*
Regression	2	34115.12	17057.56	30.78885	3.5E-08
Residual	32	17728.55	554.0173		
Total	34	51843.67			

	Coefficients	*Standard Error*	*t Stat*	*P-value*	*Lower 95%*	*Upper 95%*
Intercept	-301.461232	54.13649	-5.56854	3.8E-06	-411.734	-191.189
X Variable 1	226.5391509	29.15155	7.771084	7.31E-09	167.1594	285.9189
X Variable 2	-220.106777	30.8701	-7.1301	4.31E-08	-282.987	-157.226

This is consistent with the result obtain by I-V characteristics in A. Malshe et al [32] which states that voltage is more important for nano electro machining than current.

Higher voltages gave rise to much larger holes even with small number of pulses and thus wearing out the tip too quickly. For this reason the factorial experiments were performed with 7 V, 6 V, 5 V and this permitted time to complete the experiment before the tips were completely worn out.

Some plots in the Appendix A show the distribution of the dimensions with each repeat experiment and it is found that the consistency generally goes up as voltage is increased. It is speculated that voltages near the threshold such as 5 V or 4 V other factors such as impurities, surface texture, humidity become huge factors that contribute to the inconsistencies. It is found that the threshold for producing repeatable results is 5 V. This is established by the 3x3 experiment (with 7, 6 and 5 V and 1, 4 and 8 pulses) as discussed in the previous Section. The threshold for the actual nano electro machining is 4 V. These experiments clearly demonstrate that nano electro machining with lower voltages showed some weak dependence on the time elapsed since the previous experiment done with a higher voltage. As mentioned earlier when a hole is fabricated with one or more holes made with higher voltage a few seconds earlier produced bigger holes than those done without any prior nano electro machining within a few minutes. It is hypothesized that high voltage machining produces heat that aid low voltage machining via thermionic emission form the tip. Another hypothesis is that the high voltage causes heating of the tip which may alter the humidity or the water content surrounding it and on the surface of the sample which may have influenced the hole shape. Brooks et al [31] have hypothesized that the water content and the humidity may have played some role in the nano electro machining process.

It is not known what the exact mechanism is for material removal [31][34], hence it may not be possible to determine the reason why the voltage is more influential than the number of pulses. Field emission is the speculative process by which the electrons leave the tip [34][33] but the mechanism by which they remove material is not known.

Since the process has significant variability it would be beneficial to investigate what conditions would improve repeatability. A plot of range (difference between maximum and minimum values) of depth of holes in the factorial experiment involving 7 V, 6 V & 5 V and 4,8,12 pulses repeated four times suggest that the range of the hole dimension decreases significantly with increasing voltage. This plot is shown in plots in Figure 9 and 10. This trend is more conspicuous with the width or diameter than with depth. Thus increasing the voltage makes the process more consistent and decreases the variation in the dimensions in the holes. However the range weakly depends on the number of pulses and that increasing the number of pulses has negligible effect on the standard deviation. High voltage implies that the kinetic energy of the electrons is larger and this may overcome the effects of surface impurities and surface unevenness and other factors that may impede repeatability. Large number of pulses implies that there are more number of charge carriers with a fixed kinetic energy that may be susceptible to the factors that cause variability if they do not possess enough kinetic energy to overcome them. Thus if more consistent hole dimensions are desired then using a high voltage to fabricate them might serve the purpose.

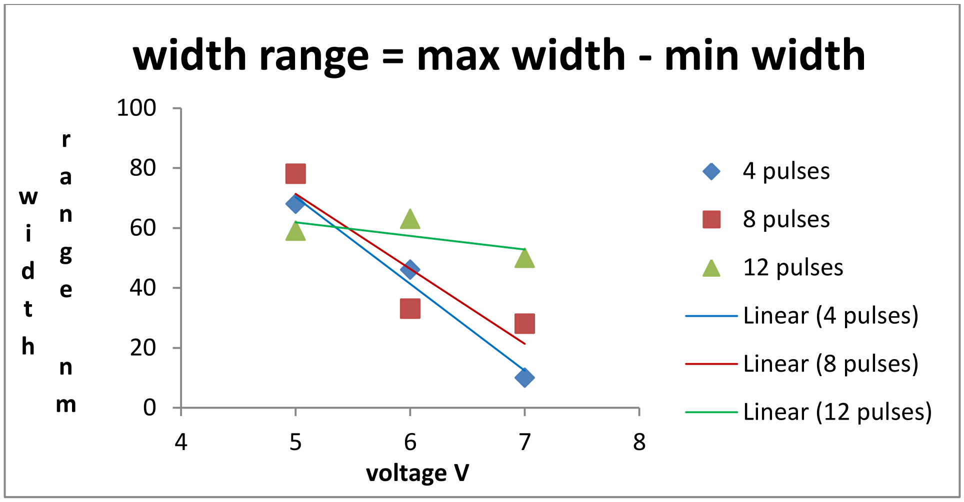

Figure 9 Shows the range (difference between maximum and minimum values) of width of holes in the factorial experiment involving 7 V ,6 V & 5 V and 4,8 &12 pulses repeated four times against the voltage.

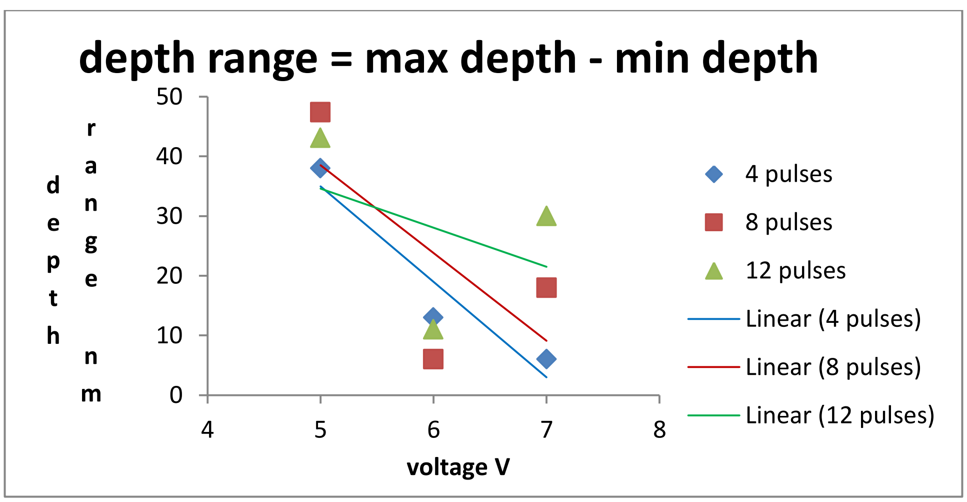

Figure 10 Shows the range (difference between maximum and minimum values) of depth of holes in the factorial experiment involving 7 V ,6 V & 5 V and 4,8 &12 pulses repeated four times against the voltage.

A plot showing all the data of the same experiment from which the standard deviation was computed can be found in Figure 19, Appendix A.

4.4 Fabrication of Slots

The aim of this experiment is to fabricate trenches or slots on the sample material. A slot was made by connecting several holes together with a small step-over distance (values are given in Table VI). The objective is to find the dependence of the dimensions of these slots on the parameters such as voltage and the number of pulses. In order to do this a 2x2 factorial experiment was performed with 6, 7 V and 4, 8 pulses. The range of voltage and number of pulses is kept relatively small as a large number of holes are to be fabricated (a slot contains multiple holes). Further an experiment to characterize the repeatability was not performed as this would require the fabrication of a large number of holes.

4.4.1 Dependence of Slot Dimensions on the Input Parameters

In this experiment, a series of holes were connected to form a trench or slot as explained in the previous Section. Figure 11 shows one such slot with 8 holes each made by 6 V and 4 pulses. The voltage and number of pulses is varied as 6, 7 V and 4, 8 pulses respectively with a 2x2 factorial experiment. For each voltage and pulse several slot were fabricated each with varying distance between the centers of holes. For some slots the distance between centers of holes may be too small making one huge hole or too large making a series of separate holes. Thus for a given voltage and number of pulses several slots were fabricated to find the distance between centers which gave the ‘best’ slot, the one with the most uniform depth and width. This ‘ideal’ distance between centers depends on the size of the holes, which in turn depend on voltage and pulses. Thus for each voltage and pulse pair the ‘best’ slot was selected for investigation.

Table IV The distances between the centers of holes that produced the ‘best’ slots (slots with fairly uniform width and depth as opposed to slots that have large spacing between holes) for a given voltage and number of pulses. It must be noted that ‘distance between two hole centers that gave the best slot’ (column 3 of table IV) is actually an output parameter found by trial and error, although it treated as one of the input parameters for making a slot. The actual output parameters are depth and width.

Table IV Input parameters used in making each slot.

Voltage for each hole in the slot	Number of pulses given to each hole in the slot	Distance between the centers of holes that gave the best slot	Number of holes in the slot
6 V	4	0.09 um	8
6 V	8	0.11 um	4
7 V	4	0.12 um	4
7 V	8	0.16 um	4

Figure 12 shows the maximum depth of a slot as function voltage and pulse. This work is limited to only four data points in case of the slots. More plots and images can be found in the Appendix A. It’s worth noting that the slots were more influenced by the number of pulses than the holes but still the voltage was the dominant factor. The 2x2 factorial experiment produces only a limited data set because the obtaining more data points would require fabricating a large number of holes as slot has more than one hole in it.

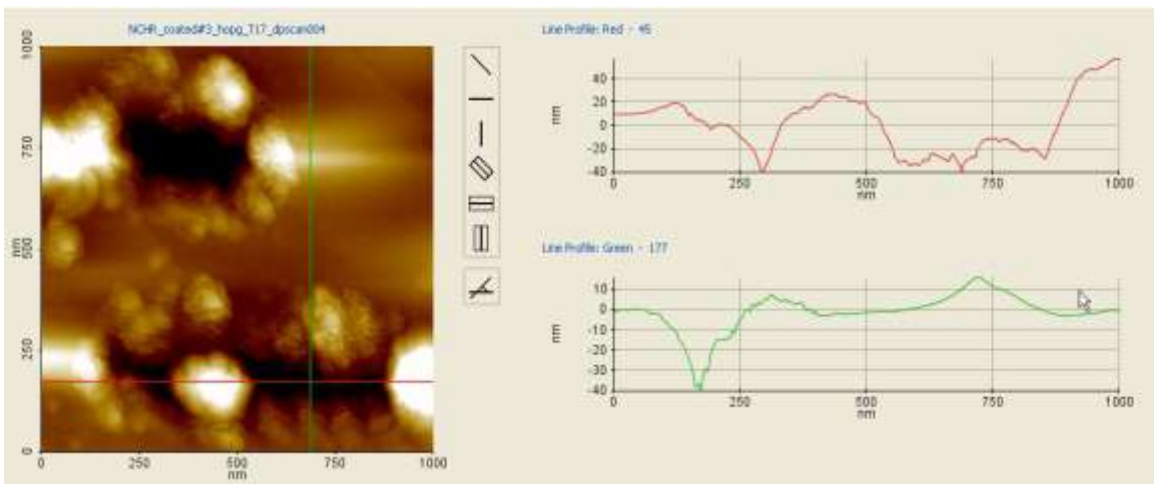

Figure 11 AFM image of a slot of 8 holes made by 6 V and 4 pulses each. The other slot is made by 6 V and 8 pulses.

The data here is seemingly far more consistent than the results shown in the previous Section as there are a small number of data points and these produce straight lines. The depth in Figure 12 refers to the maximum depth as there is some variation of depth in the slot along its length. Figure 12 also shows some variation in the width because a slot is made from multiple holes. This experiment may establish the fact that it may be feasible to make trenches made from connecting holes together. And one can expect the dependence of the dimensions on the input parameters to be somewhat consistent with that of stray holes discussed in the previous Section.

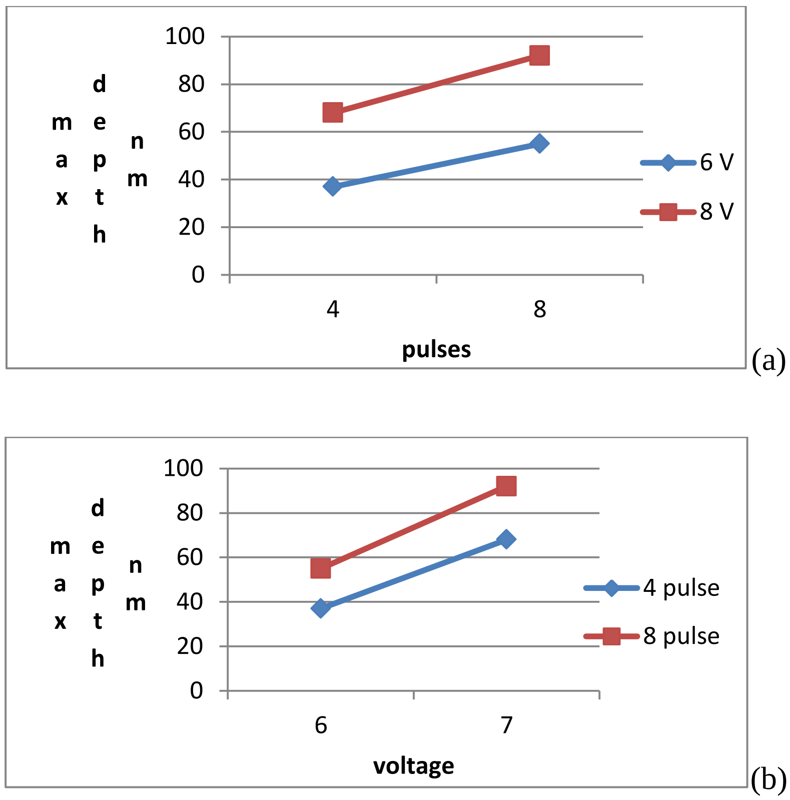

Figure 12 (a) Plots of max depth vs. number of pulses for each voltage and (b) plot of max depth vs. voltage for each pulse.

4.5 Hole Dimension Variation Using a Nano-wire Electrode

The aim of this experiment is to determine the effect of a change in the aspect ratio of the tip on the dimension of the holes and to assess the feasibility of using a nanowire as an electrode. To perform this experiment a poly-crystalline silver nano-wire is soldered to the standard tip with an epoxy and coated with a total thickness of 40 nm to 60 nm of gold and palladium by sputtering. Using this tip an experiment similar to the one described in Section 4.1 was performed. The nanowire is made of poly crystalline silver and is around 3-4 um in length and about 100+ nm in diameter. Some SEM images of the nanowire can be found in Appendix D. The nanowire was soldered to the standard tip using an epoxy. It was coated with gold and platinum to improve the conductivity at the soldered area as the epoxy is non-conducting. The cantilever used was a contact-mode cantilever as a non-contact cantilever damaged the nanowire whenever it was used for imaging. The set point was small (0.03 nN) to protect the delicate nanowire. The voltage to the tip was also kept deliberately low to protect the nanowire. This experiment is very similar to the one described in Section 4.1 with the only major difference being the aspect ratio of the AFM tip. The details of the parameters that were used in this experiment are given in Table IV.

In order to determine the dependence of the hole dimensions, just like for the standard tip, two factorial experiments were performed. One was a 3x3 with 4, 4.5 and 5 V and 2,4 and 8 pulses and the other was a 1x5 factorial with 1,2,4,8 and 12 pulses at 4 V. The purpose of 1x5 factorial experiment was to investigate the influence of large number of pulses at a constant voltage. Figure 13 shows the AFM image of three holes from the 1x5 experiment. Figure 14 show the dependence of depth on voltage in the 1x5 experiment. More plots can be found in the appendix A. The aim of the 1x5 experiment was to show the influence of a large range of pulses at a constant voltage. The aim of the 3x3 experiment was to show the influence of a small range of voltage for each number of pulses. The 1x5 experiment shows a fairly consistent increase in the depth as well as the width with respect to the number of pulse.

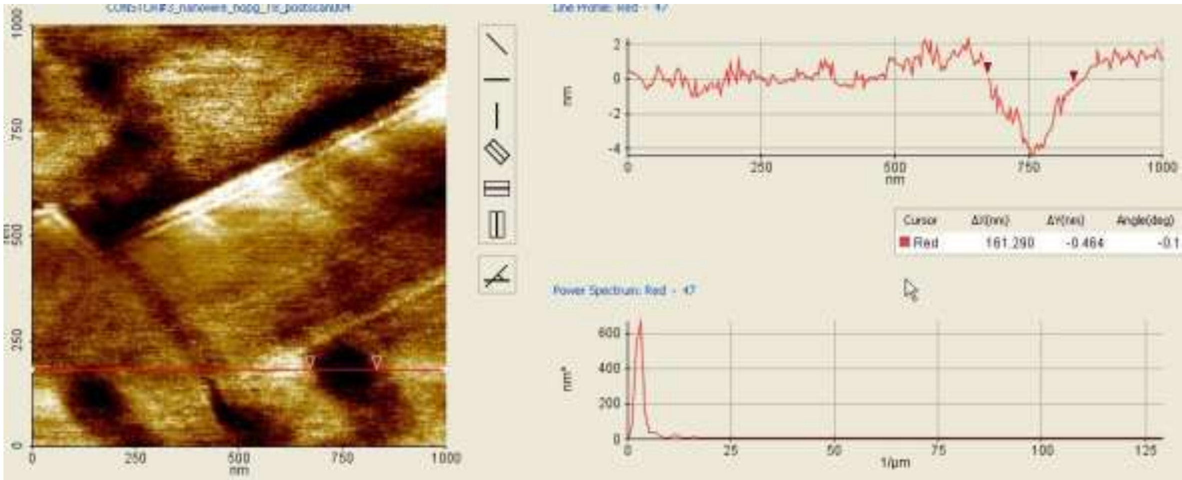

Figure 13 AFM image of three holes made with 4 V each and varying pulses.

The dependence on number of pulses is seemingly better than the ones obtained with the standard tip in Section 4.2 and 4.3. A standard tip is observed to be non-repeatable at 4 V while the nano-wired tip shows a dependence on number of pulses at 4 V which is as consistent as the one in Section 4.3. The 3x3 experiment however shows some inconsistency as the removal rate reduced significantly at higher voltage. The cause of this may well be tip wear. Nano electro machining completely ceased after the experiment at all voltages and thus it is speculated that the gradual tip wear contributed to less material removal upon reaching the high voltage limit of the experiment. The nanowire nonetheless showed a gradual increase in dimension with increase in voltage before the wear started to occur which was at about 4.5 V. It can be concluded that the nanowire is indeed feasible and apparently more consistent than the standard tip. A longer nanowire can be used to improve the tool life although a long nanowire may be prone to mechanical damage while scanning.

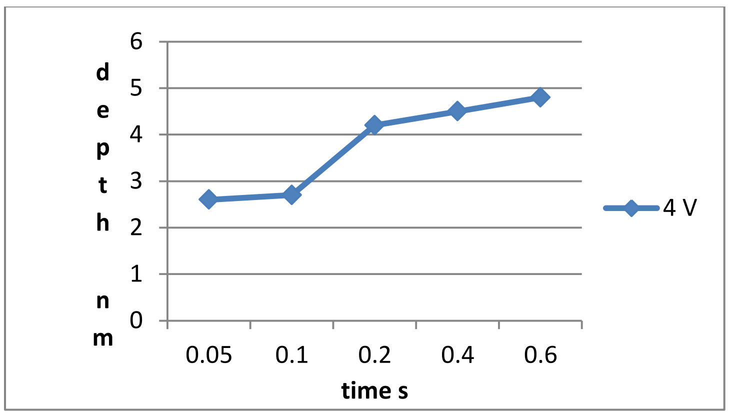

(a)

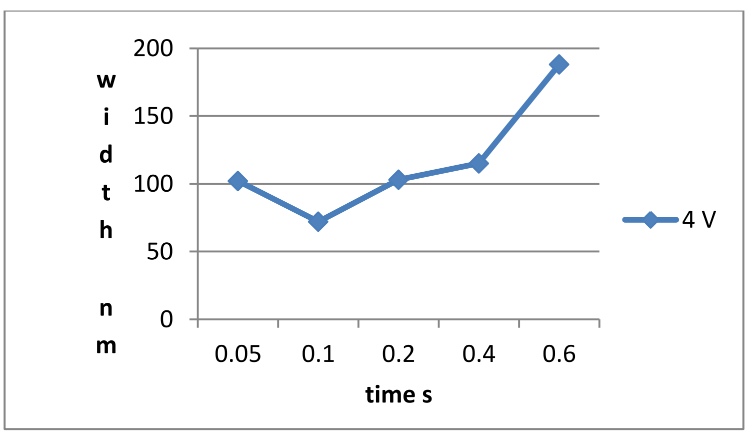

(b)

Figure 14 (a) Plot of width(diameter) of the resulting hole when using the nanowire against number of pulses for 4 V. (b) Plot of depth of the resulting hole when using the nanowire against number of pulses for 4 V.

The other observation from this experiment is that the holes made from the nano-wire seem to be shallower than those made by the standard tip, most likely due to the difference in aspect ratio. A discussion regarding this is given in the next section.

4.6 Explanation of Different Hole Shapes Arising Due to Different Tip Geometries

The purpose of this model is to explain a significant difference in dimensions of the holes fabricated by the standard tip and the nano-wire tip. It may be surmised that the geometry or aspect ratio of the tip may have a significant impact on the dimensions of the holes. The difference in dimensions of the holes fabricated by the tips is given below in the table V. The contact area between the tip and the sample should be similar in case of both tips i,e nanowire and the standard tip.

Table V Experimental data showing the differences in the dimension of holes made by two tips of different aspect ratios with same voltage and number of pulses. The sample was HOPG.

Voltage given to the tip(V)	Number Pulses given to the tip	Resulting hole made by Standard tip- low aspect ratio	Resulting hole made by Nanowire- high aspect ratio	Width difference between the two holes	Depth difference between the two holes
4	1	Depth = 1 nm width = 25 nm	Depth = 2.3 nm width = 103 nm	78 nm	1.3 nm
4	2	Depth = 0.5 nm width = 24 nm	Depth = 2.4 nm width = 72 nm	48 nm	1.9 nm
4	4	Depth = 0.8 nm width = 20 nm	Depth = 4.2 nm width = 104 nm	84 nm	3.4 nm

. This is because both tips are curved at the end with a similar radius of curvature which is estimated to be around 100 nm (200 nm in diameter) for the nanowire and 80 to 100 nm (160 to 200 nm in diameter) for the standard tip (30 to 50 nm in the original case, presumably increased to 80 or 100 nm after 40 to 60 nm of coating with gold and palladium by sputtering). SEM images of standard tip as well as the nanowire tip can be found in Appendix D. As the radii of curvature are very similar, the dimensions of the resulting holes for the two tips should not vary much for the same conditions. However, the experiment reveals that the average width (diameter) difference of the resulting holes is around 70 nm and the average depth difference is around 2.2 nm for the two tips under the same conditions.

One explanation is that the shape difference of the two tips causes a difference in the distribution of the electric field which in turn causes the electrons to be distributed differently with both tips thereby causing the vast width difference and relatively depth difference. The average aspect ratio (width/depth) is similar for both cases because of the some inconsistency with one of the holes made by the nanowire. If one looks at the average aspect ratios of the both tips they may look similar (around 32 for both cases) one might think dimensions of the holes do not differ much, but this perspective obscures the reader of the massive width difference between the holes made by two tips of similar radius of curvature (but different geometries).

The explanation of this phenomenon by the mere difference of electric field distributions does not accurately fit the picture as electrons are ejected by means of Fowler-Nordheim tunneling. Nearly all the work done using this nano electro machining process have cited

Fowler-Nordheim tunneling as a possible mechanism that contributes to hole formation [31 to 34]. Thus the Fowler Nordheim tunneling must also be taken into account in addition to the electric field distribution.

The single particle Schrodinger equation is associated with the electrons that pass through the tip and proceed towards the sample material for nano electro machining. The reason for using the Schrodinger equation for this that it is the only model that predicts tunneling as no classical theory does so. The Hamiltonian in the Schrodinger equation is for a single particle in a time-independent potential. There is no seemingly plausible reason to take into account interaction effects and spin. The potential is treated time-independent to keep the model simple when in reality, it is a pulse. Further, this is a three-dimensional problem due the nature of the AFM tip. The solution of a 3-D problem may possess spherical harmonics with a complicated 3-D potential thereby making the solution inherently complex. This prompted the Schrodinger equation to be solved as a one-dimensional one to keep the model as simple as possible.

The Schrodinger equation is shown below.

$$H \mid \Psi >= E \mid \Psi >$$

The H in the above equation refers to the single-particle Hamiltonian of the electron. The Hamiltonian here is the sum of kinetic energy and the potential experienced by the electron from electric field applied to the tip. The Psi refers to the single-particle wavefunction of the electron leaving the tip and E is the energy Eigen value.

To make the calculation as simple as possible the following assumptions are made:

1. Single particle, the Hamiltonian contains only one particle
2. The electron-electron interaction term in Hamiltonian is ignored
3. Space states only, spin states are ignored
4. Time independent, time dependence is ignored
5. One dimensional, this keeps the calculation as simple as possible

The potential in the Hamiltonian corresponds to the potential around the tip. This potential is uniform in case of a sphere and varies in case of a cone (or any geometry without spherical symmetry).Though the potential is a square wave-pulse, it assumed to be a constant in time to keep the model as simple as possible. When solved, the solution wavefunctions would represent the probabilities (after taking the complex modulus of the wavefunction) of the spatial locations. In a simple 1-D problem, there are two probabilities: getting transmitted and reflected through the barrier potential. It is classically impossible for electrons to travel through a barrier potential whose magnitude is greater than the kinetic energy; hence they tunnel through. The transmission coefficient represents the fraction of electrons that tunnel through as opposed to the ones that get reflected. When the 1-D Schrodinger equation above is solved using some trial wavefunctions the transmission coefficient can be obtained as a function of energy and potential. Thus, in this case, the transmission coefficient represents the number of electrons that are ejected out of the tip as a function of the electric field experienced by the electrons. The solution is obtained for an arbitrary potential and the transmission coefficient thus obtained is shown below. The details of this calculation are given in the appendix E.

$$TC = exp(\frac{-2}{h}\int_0^{W^{-1}(\phi-E)} \sqrt{2m(W(x)+\phi-E)}dx)$$

The above equation is derived from the solution of the schroedinger equation. The TC in the above equation refers to the transmission coefficient (probability or fraction of electrons that ejected or tunneled out of the AFM tip). W(x) is the potential experienced by the electron due to the applied electric field, x is the distance from the surface of the tip, E is the energy at which the electron approach the surface of the tip from inside the tip (to be tunneled out) and this usually the Fermi level and phi is the workfunction of the material or energy required to draw out the electron from a material.

In the case of Fowler-Nordheim tunneling or field emission, as is the case here, the transmission coefficient would only depend on the electric field and not the distance between tip and sample. This means that probability of tunneling (or the number of electrons ejected from the surface) increases when the electric field strength increases.

Here it is attempted to establish the distribution of the transmission coefficient around the tip. The electric field strength any given location around an AFM tip must vary due to the geometry of the tip and this variation must differ with different tip geometries i.e. the standard tip and nanowire. If the electric field distribution around the tip varies according to the tip aspect ratio then so should the transmission coefficient. The variation of transmission coefficients for different tip aspect ratios must explain the difference in hole dimensions produced by the two tips if Fowler-Nordheim tunneling plays a role in nano electro machining. This explanation of variation of hole dimensions for the two tips by means of the difference in transmission coefficient distribution is the entire goal of this model.

In the equation for the transmission coefficient, the arbitrary potential is substituted with the potential experienced by the sample in presence of the tip, details of which are given in Appendix E. As this is a 1-D problem, the potential, which has azimuthal symmetry, is treated as 1-D in the radial direction and the angular part is treated as a constant throughout. Both the radial part and angular part differ for the different tips. The different potentials (electric field is the gradient of potential by definition) for the different tips are plugged in the expression for transmission coefficient. For illustrative purposes, the transmission coefficient is plotted as a function of the horizontal distance on the sample from directly under the center of each tip (Figure 15 (a) and (b)). It was difficult to exactly calculate the potential and/or electric field experienced by the sample due to absence of certain numerical boundary conditions such as surface charge distribution. The details are given in Appendix F and in [37] and [39]. These constants are assigned arbitrary values and hence the model only serves to show the difference in trend of the distribution of transmission coefficients (or the squares of which) between the two tips. Figure 15 (a) shows the plot of the trends in squared transmission coefficients for the standard tip and nanowire. The figure also depicts how the two tips are treated in order to obtain the difference in electric field distributions.

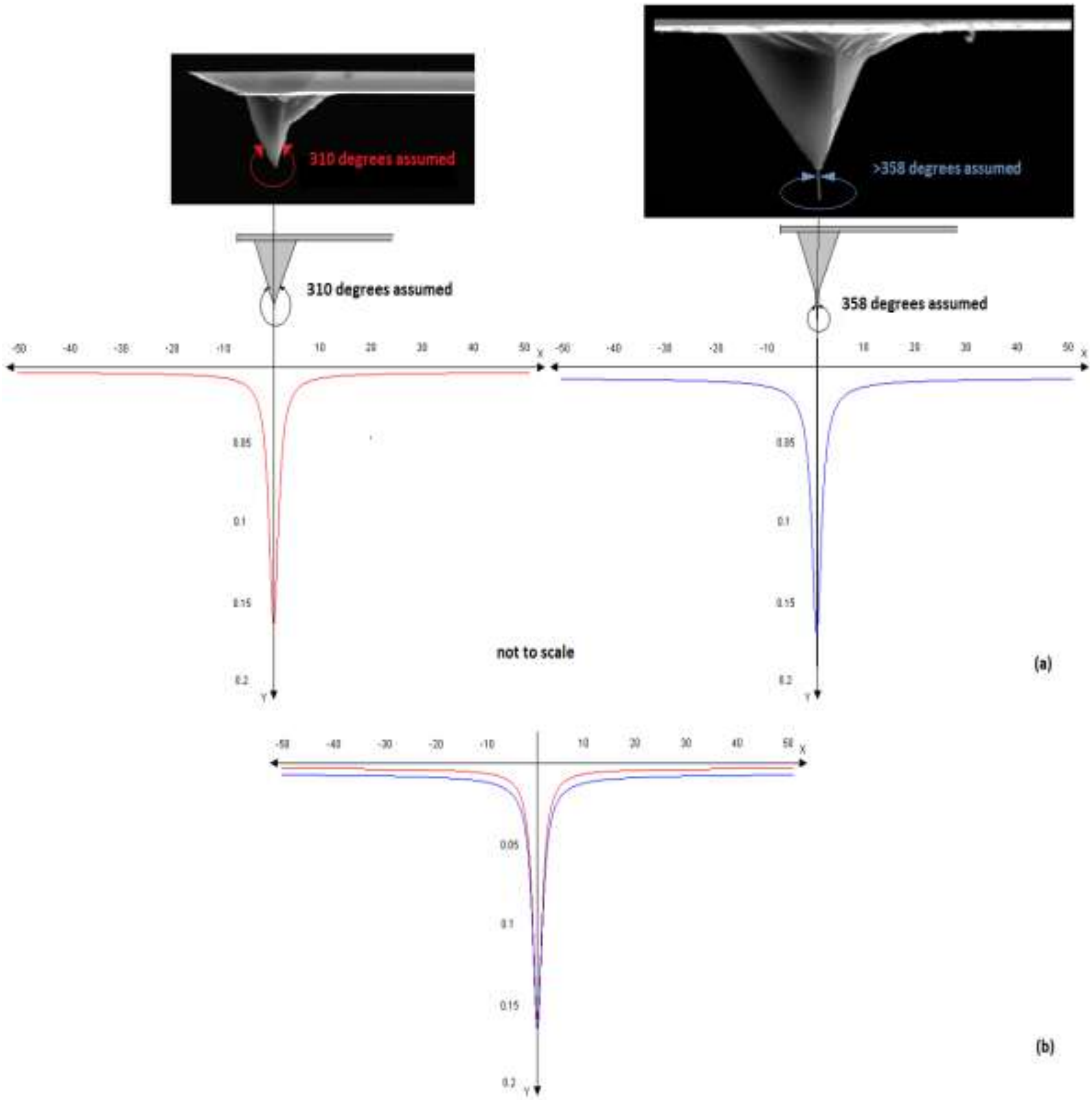

Figure 15 (a) The schematic representation of the trends of the distribution of the squared transmission coefficient for both the standard tip and the nanowire tip. For the sharper tip the distribution on the flat surface broadens (depicted more clearly in Figure 15 (b)). The y-axis is the transmission coefficient and the x-axis can be thought of as the same surface relative to the location of the tip. (b) The distribution of squared transmission coefficients of the standard tip (red) and nanowire (blue) are plotted in the same graph. The x-axis represents the location on the flat sample surface. The origin represents the point directly underneath the center of the tip.

The standard tip is cone with 50 degree characteristic cone angle while the nanowire is cone with <2 degrees characteristic angle. Ideally, a wire is a cone with 0 degree characteristic angle, but here it is arbitrarily given a small angle to demonstrate how the electric field and subsequently the transmission coefficient vary towards that limit. For a better interpretation the plots are overlapped in Figure 15(b). The y-axis in this figure shows the transmission coefficient relative to the horizontal distance on the sample. The origin is the point on the sample directly under the center of the AFM tip. It is to be noted that the transmission coefficient is plotted as function of horizontal distance. This quantity is maximum at the center where the electric field is strongest. When moving away from the center, the coefficient decreases as the field strength decreases. This decrease is faster for the standard tip than the nano-wired tip. If the material removal rate depends directly on the squared transmission coefficient, then the width of the hole corresponds to point on the x-axis when the transmission coefficient is nearing zero.

When the transmission coefficient nears zero it means that fraction of electrons ejected at that location is nearly zero and nano electro machining will cease to occur. The plot in Figure 15 is plotted upside down for illustrative purposes. For the same arbitrary values of constants in the expression, the value of the transmission coefficient (number or fraction of ejected electrons) for the nanowire at 100 nm is equal to the value of transmission coefficient for the standard tip at 25 to 40 nm (see Figure 15). So the difference in width for the two cases must be around 60 to 75 nm under the same conditions. This, to some extent, agrees qualitatively with the experiment in Table V. There is no significant difference in the transmission coefficient (number or fraction of ejected electrons) at the point directly under the tip, meaning the maximum depth isn't significantly different for each case. This also agrees with experiment in Table V where, the average difference in depth is around 2 nm, which is small or negligible compared to the large average width difference of 70 nm for the two different tips (Table V). However, the model depicts holes which are deeper at a width less than 10 nm than the actual experiment in Table V for both the tips. This disparity could be due to the fact that there is no clear connection between the transmission coefficients and the amount of material removed. The transmission coefficient only represents the fraction of electrons ejected from the surface and not the actual material removed.

This model illustrates the role of Fowler-Nordheim tunneling in influencing the shape of holes made by tips of different aspect ratios. The tunneled electrons increase at the areas where the electric field strength is high which is to some extent reflected by experiment. However, Fowler-Nordheim tunneling may only be a part of the mechanism and the model only suggests how the electrons leave the tip but not how they impact the sample. This again raises the issue of the dearth of knowledge of the mechanism involved in removing the material. There may be other processes that explain the material ejection by the electrons which when combined with the Fowler-Nordheim tunneling model may establish a broader picture of the physics behind the process.

4.7 Comparison with Other Results

Many experiments using the nano electro machining have been performed in various conditions and materials and tips. Conditions include air as well as a dielectric medium, substrates include gold as well as HOPG and tips may be nanowire, standard tip and carbon nanotube. All of these produced different results in terms of output parameters such as hole size and input parameters such as tip shape, voltage and machine time or number of pulses. The chief output parameter is the material removal rate or the amount of material removed per unit time under certain conditions such as voltage, or substrate material etc. The table VI below shows a comparison of various material removal rates under various conditions.

Table VI Various material removal rates for various experiments

work	Tip	Sample	Medium	voltage	Max Pulses	Geometric assumptions	Material removal rate (cu. Nm/s)
This work	Standard tip	HOPG	Air	7 V	12	Cone	150000
This work	Nano wire	HOPG	Air	4 V	12	Cone	64000
[32]	Standard tip	gold	Dielectric	10 V	4500	V-shape	141
[31]	Standard tip	HOPG	Air	10 V	1000	unspecified	280

The medium is air or dielectric with substrate being HOPG or a metal with varying voltage. Clearly more experiments under various combinations of conditions are needed to determine the nature of the material removal mechanism and to quantify its dependence on the various conditions. The huge difference may be attributed to the difference in removal rates arising due different mechanism in the atomic scale. The nano electro machining done under the dielectric medium could be due either bond tunneling or space tunneling or combination of the two [32]. The one done in air can be only subject to space tunneling. Also the material removal rate difference can also be attributed to difference in sample material with HOPG being layered hexagonal structure and gold being FCC. The crystal structure and bonding may influence the rate at which atoms are separated. Also the difference in material removal rate between the nanowire and the standard tip can be because of the operating voltage. The voltage of the nanowire has been deliberately kept low to protect the delicate structure. Further, the shape and electric potential distribution mentioned earlier may influence the total or effective material removed per pulse. There is a considerable difference in material removal rate using a standard tip on HOPG with 10 V done by Brooks et al [31]. The removal rate there is considerably smaller under similar condition than the one done here. Though the experiment is done under similar conditions the material removal rate is around 500 times higher in this work. This discrepancy can be explained as follows. The geometric assumption made in calculating the volume differs greatly in both works. The cone approximation for calculating the volume (used in this work) yielded a volume around 6 times higher than the work by [31] for the same values of diameter(width) and depth of hole). Further for similar number of pulses (10 to 20 seconds) the volume (calculated by the cone approximation) yielded a volume of material removed 500 to 3000 times higher for this work than that for [31]. When nano electro machining was done 1000 to 2000 pulses with 6 to 8 V yielded very large holes and reduced the lifetime of the tip (these results are not shown here). The combination of difference in geometric assumption and the larger material removal attributed to the large removal rates for both works. The large difference in material removal between both works can be due to differences in humidity and more importantly difference in proper (or improper) electrical contact within the circuit which may lead to more (or less) energy transferred the tip from the signal generator. The equipment used in this work may have admitted the pulse from the signal box with very little loss as there was a provision in the AFM system for exactly such a purpose. Thus it may be sound to perform experiments which involve drastically different conditions with the same equipment rather than to compare data from different sources.

In addition the work done by Park et al [34], the holes made by the carbon nanotube were much deeper than the ones with the standard tip. In the work here it was the opposite as the holes made by the nanowire were shallow. The disparity here may be explained by the difference between the carbon nanotube and the nanowire. The nanowire used here is single crystal wire of silver coated with gold and palladium and it is assumed to be completely isotropic. The multi walled carbon nanotube however may have anisotropic electrical conductivity. Vertically aligned single walled carbon nanotubes have shown to have anisotropic electrical conductivity with the conductivity along the length being around 23 to 60 times higher than that along the diameter [35].

5. CONCLUSION AND FUTURE WORK

Nano electro machining was performed on a HOPG substrate as well as aluminum using an Atomic Force Microscope with negative pulses (4 V to 7 V) using a tips with different aspect ratios. Factorial experiment with voltage and machining time were performed. Experiments with the tips with different aspect ratios were performed. Further other features like slots were fabricated and similar 2x2 factorial experiment was performed for the slots. A simple model was constructed in an attempt to explain the dimensional differences in the feature involving the nanowire tip and the standard tip. The key conclusions can be summarized as follows:

- Voltage is the chief factor that influences nano electro machining at the nano scale
- The threshold voltage for material ejection is 4 V while that for repeatability is 5 V
- The process is somewhat repeatable but not to a great extent owing to variations in surface texture, impurities, humidity and temperature.
- The dimensions of resulting holes (width(diameter) and depth) are best modeled by logarithm of voltage and number of pulses (depth or width(diameter) = ln(PV) + ln(P))
- When doing an experiment with this process using multiple voltages, it is most advantageous to start with the highest voltage.
- The electric field distribution around the tip influences the shapes of the features by increasing the amount of Fowler-Nordheim tunneling at the places of high electric field thereby increasing the material removed.

- Fowler-Nordheim tunneling plays a role (explains how electrons leave the AFM tip) but does not completely describe the material removal mechanism (more work to be done on how the electrons that left the AFM tip remove the material).

Differences in the sample, nano electro machining environment and equipment differences (different AFM) play a significant role in influencing the material removal rate as may temperature and humidity.

The immediate future work would be to perform an experiment to see if the set point has any influence on the dimensions of the features. It may be very sound to perform an nxn experiment with voltage and set point. The experiment can also be performed under different environments and different substrates with the same equipment to quantify the one with the most influence. The model mentioned above can be given a more accurate picture of the electric potential and field distribution around the tip. The model can also be significantly improved to overcome its shortcomings. Also more improvements can be given to the model to predict the material removal rate for different materials by expanding it to include the nature of the material. More models can be proposed to establish the relationship between the material removal mechanism and the transmission coefficients. In a broader perspective, Silicon can be doped and electro-machined for the first time. Further, with the knowledge from this work, other work and any future work can be utilized to use this process in a non-SPM context. Imprints, for example, may be utilized to fabricate the anti-dot array, like the one made here, in a much quicker way. This facilitates much faster fabrication of the plasmonic devices. The first device fabricated using this process would establish this process as an important fabrication technique in the semiconductor industry.

REFERENCES

1. Douglas M. Photiadis, J. A. Bucaro, and X. Liu, (2006). “Quantum statistical effects in nano-oscillator arrays”, *Physical review*, B 73, 165314 _2006.

2. M. Lazara, H. Vanga, P. Brosselard, C. Raynaud, P. Cremillieu, J. L. Leclercq, A. Descamps, S. Scharnholz, and D. Planson, (2006). “Deep SiC etching with RIE”, *Superlattices and Microstructures,* 40, 388-392.

3. E.M. Bringa and R.E. Johnson, “Sputtering of nano-grains by energetic ions”, *Nuclear Instruments and Methods in Physics Research*, B 193 (2002) 365–370.

4. O. D. Potapkin and B. V. Troshin, (2010). “Projection Electron Beam Lithography for Nanotechnology”, *Bulletin of the Russian Academy of Sciences: Physics*, Vol. 74, No. 7, pp. 1015–1019.

5. R. Tanabe, Y. Ito, H., Takezawa and N. Mohri, (2005). “Time-resolved observation of the change of electrode shape in single discharge: rapid self-forming of a thin electrode”, *Journal of Applied physics*, 97, 5, 53301-53301.

6. S. Osakoy, T. Sugiharaz, Y. Yamamotoz, T. Maemotoz, S. Sasaz, M. Inouez and C. Hamaguchi, (1996). “Quantum anti-dot arrays and quantum wire transistors fabricated on InAs/Al0:5Ga0:5Sb heterostructures”, *Semiconductor Science and Technology*, 11 (1996) 571–575.

7. Milhiet P-E, Yamamoto D, Berthoumieu O, Dosset P and Le Grimellec C, (2010). “Deciphering the Structure, Growth and Assembly of Amyloid-Like Fibrils Using High-Speed Atomic Force Microscopy”, *Public library of science ONE*, 5(10): e13240.

8. M. Jastrzebska, I. Mro´z and B. Barwin, (2010). “AFM investigations of self-assembled DOPA–melanin, nano-aggregates”, *Journal of Materials Science*, 45:5302–5308.

9. N. Yilmaz, S. Ida and Y. Matsumoto ,(2009). “Electrical conductivities of nanosheets studied by conductive atomic force microscopy”, *Materials Chemistry and Physics*, 116 (2009) 62–66.

10. J. Yaminsky and V. Igor, (1999). "Magnetic force microscopy", *Russian chemical reviews*, (0036-021X), 68 (3), p. 165.

11. Y. F. Dufrene ,(2008).”AFM for nanoscale microbe analysis”, Analyst, 133, 297–301.

12. Avouris, P., Hertel, T. and Martel, R., (1997). *Applied Physics Letters*, 71, 285-287.

13. S. W. Park and C. F. Quate, (1995). "Nanometer scale lithography at high scanning speeds with the atomic force microscope using spin on glass", *Applied Physics Letters*, 67 (16).

14. S. W. Park and C. F. Quate, (1995). "Nanometer scale lithography at high scanning speeds with the atomic force microscope using spin on glass", Applied Physics Letters, 67 (16).

15. F. C. Simeone, C. Albonetti, and M. Cavallini ,(2009). "Progress in Micro- and Nanopatterning via Electrochemical Lithography", *Journal of Physical Chemistry*, 113, 18987–18994.

16. R. Garcia, R. V. Martinez and J. Martinez, (2006). "Nano-chemistry and scanning probe nanolithographies", *Chemical Society Reviews*, 35, 29–38.

17. M. Wendel , (1996)."Nanolithography with an atomic force microscope", *Superlattices and Microstructures*, Vol. 20, No. 3.

18. U. Kunze, (2002). "Nanoscale devices fabricated by dynamic ploughing with an atomic force microscope", *Superlattices and Microstructures*, Vol. 31, No. 1.

19. A.J.M. Giesbers , U. Zeitler , S. Neubeck, F. Freitag , K.S. Novoselov and J.C. Maana, (2008). "Nanolithography and manipulation of graphene using an atomic force microscope", *Solid State Communications*, 147 (2008) 366–369.

20. *Technology Review*; Jan/Feb 2009, Vol. 112 Issue 1, p84-85, 2p.

21. A Notargiacomo, V Foglietti, E Cianci, G Capellinik, M Adami, P Faraci, F. Evangelistik and C Nicolini, (199). "Atomic force microscopy lithography as a Nano device development technique", *Nanotechnology*, 10 (1999) 458–463.

22. B. A. Gozen , (2010). "A Rotating-Tip-Based Mechanical Nano-Manufacturing Process: nano-milling", *Nanoscale Research Letters*, 5:1403–1407.

23. C. H. Park, S. Bae and H. Lee, (2006). "Nano-oxidation of Si using ac modulation in atomic force microscope lithography", *Colloids and Surfaces A: Physicochemical Engineering Aspects*, 284– 285, 552–555.

24. R. V Martınez, J. Martınez and R. Garcia, (2010), "Silicon nanowire circuits fabricated by AFM oxidation nanolithography", *Nanotechnology,* 21, 245301 (5pp).

25. P. Scheier and K. Sattlera, (2003). "Scanning tunneling lithography of silicon nanoparticle films", *European Physical Journal*, D 24, 347‑349.

26. T. Osada, N. Zhu, Y. Zhang, and T. Komeda, (2008). "Molecule-Precision Cavity Formation in Molecular Layer Using Scanning Tunneling Microscope Lithography", *Journal of Physical Chemistry*, C 2008, 112, 3835-3839.

27. C.R.K. Marrian and E.A. Dobisz , (1992). "Scanning tunneling microscope lithography: a viable lithographic technology?", *Society of Photographic Instrumentation Engineers*, Vol. 1671 (1992).

28. D.T. Pham, S.S. Dimov, S. Bigot, K. Popov, (2004), *Journal of Materials Processing Technology*, 149, 50-57.

29. A. D. Farson, H. Choi, and S. Rokhlin, (2006). "Electrical discharges between platinum nanoprobe tips and gold films at nanometer gap lengths", Nanotechnology, 17,1, 132-139.

30. K.P. Rajurkar, G. Levy, A. Malshe, M.M. Sundaram, J. McGeough, X. Hu, R. Resnick, and A. DeSilva, (2006). "Micro and nano machining by electro-physical and chemical process", *Annals of CIRP*, volume 55 2/2006.

31. J.G. Park, Q. Lui, C. Zhang, R. Liang, B. Wang, J. Pignatiello, J. Brooks, K. McBrearty, R. Wysk and P. Cohen, (2006). "Electro-Machining (EM) using metal coated atomic force microscope tip and single-walled carbon nanotube bucky-paper", *FILMS Proceedings of MN 06*: *6th Multifunctional Nanocomposite International Conference* Sept. 20-22, 2006, Honolulu, Hawaii.

32. A. Malshe, K. Virwani, K.P. Rajurkar, and D. Deshpande, (2005). "Investigation of Nanoscale electro-machining in dielectric oil", *Annals of the CIRP*, volume 54 1/2005.

33. K. Virwani, A. Malshe and K.P. Rajurkar, (2007). "Understanding dielectric breakdown and relative tool wear characteristics in nano-scale elector machining", *Annals of CIRP* ,volume 56 1/2007.

34. J. G. Park, C. Zhang, R. Liang and B. Wang, (2007). "Nano-machining of highly oriented pyrolytic graphite using conductive atomic force microscope tips and carbon nanotubes", *Nanotechnology*, 18 (2007).

35. C. T. Lin, C.Y. Lee, T. S. Chin , R. Xiang , K. Ishikawa ,J. Shiomi and S. Maruyama, (2011). "Anisotropic electrical conduction of vertically-aligned single-walled carbon nanotube films", *Carbon 49*, 1446-1452.

36. A. Messiah (1991), “Quantenmechanik 1”, *DeGruyter*, 1991.

37. R. N. Hall, (1949). “The Application of NonIntegral Legendre Functions to Potential Problems”, *Journal of Applied Physics,* 20, 925.

38. B. H. S. Fricker, (1989), “Why does charge concentrate on points?”, *Physical Education,* 24 .

39. D. Jackson, (1999). “Classical electrodynamics”, 3rd edition*, John Wiley & sons Inc*.

40. G. Squires, (1995). “Problems in quantum mechanics”, *Cambridge University Press*, Cambridge. UK.

APPENDIX

A. Additional Results from HOPG Experiments

The following plots are results from various experiments in addition to those shown in Sections 4.1 through 4.6 in Chapter 4. The following plot in Figure 16 corresponds to the average width of resulting holes from the 3x3 factorial experiment (number of pulses 1,4,8 and voltage 7 V, 6 V, 5V) which was repeated four times as described in Section 4.2.

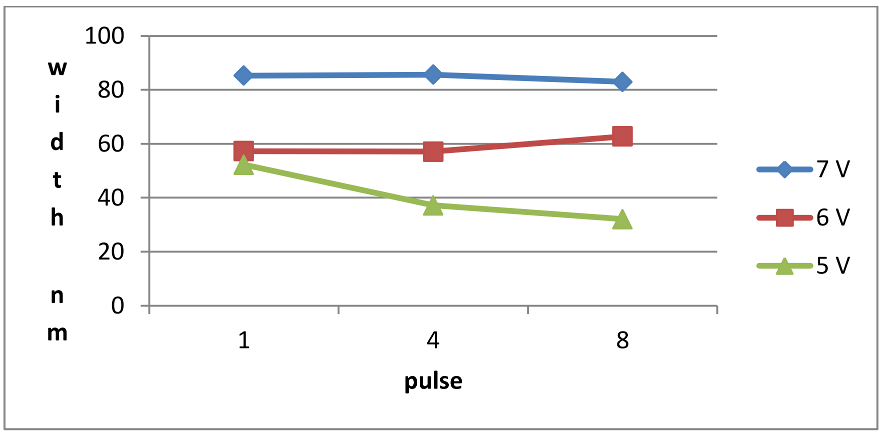

(a)

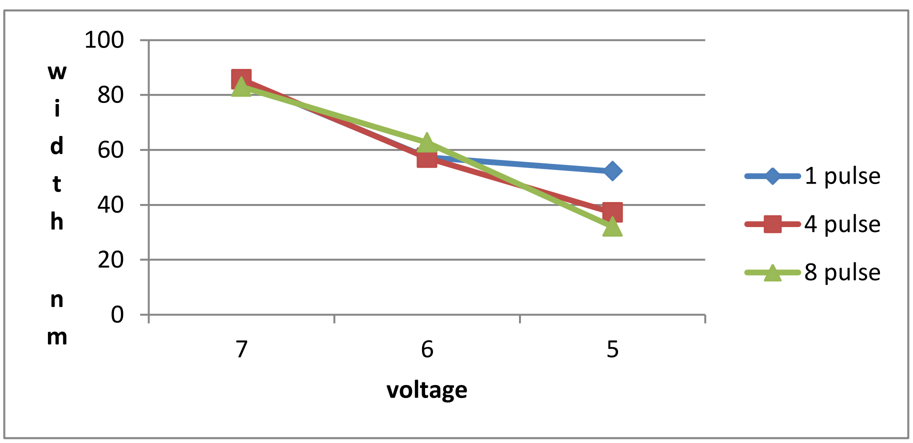

(b)

Figure 16 The average width dependence for an experiment done with 7 V, 6V and 5 V and 1,4,8 pulses on (a) pulse for each voltage and (b) voltage for each pulse.

The plot in Figure 17 depicts average width of resulting holes from a 3x3 factorial experiment (number of pulses 1,4,8 and voltage 7 V, 6 V, 5V) which was repeated four times as described in Section 4.3).

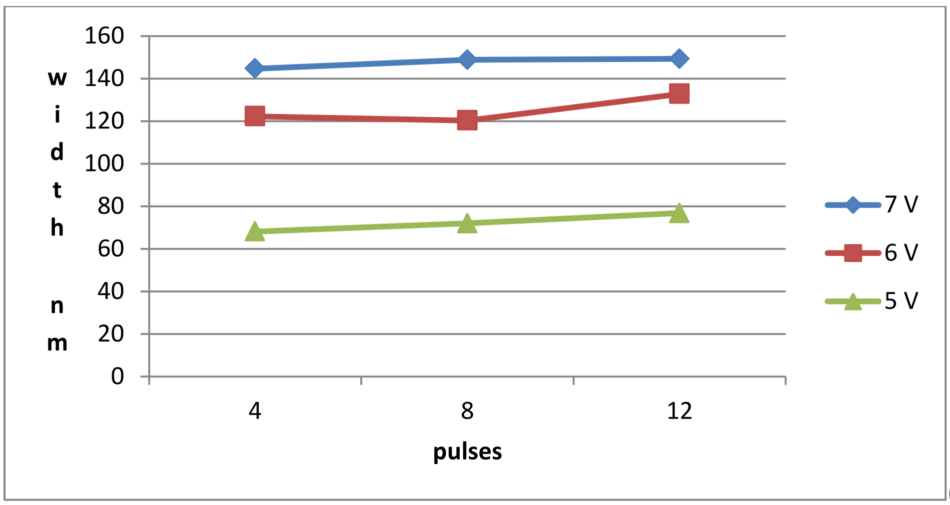

(a)

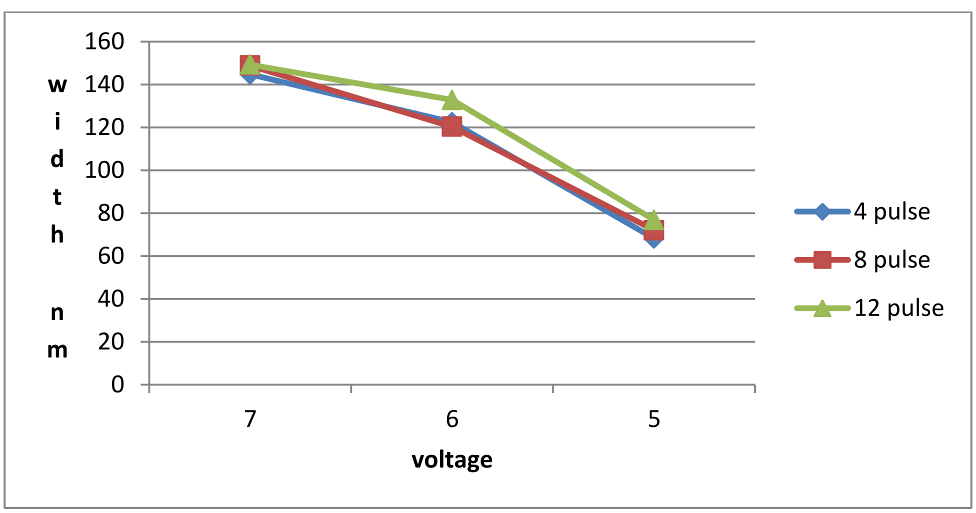

(b)

Figure 17 The average width dependence for an experiment done with 7 V, 6V and 5 V and 4,8,12 pulses on (a) pulse for each voltage and (b) voltage for each pulse.

The plot in Figure 18 depicts width of resulting holes from a 12x3 factorial experiment (number of pulses 1,2,4 and voltage 4V to 9.5 V) which was repeated four times as described in Section 4.3).

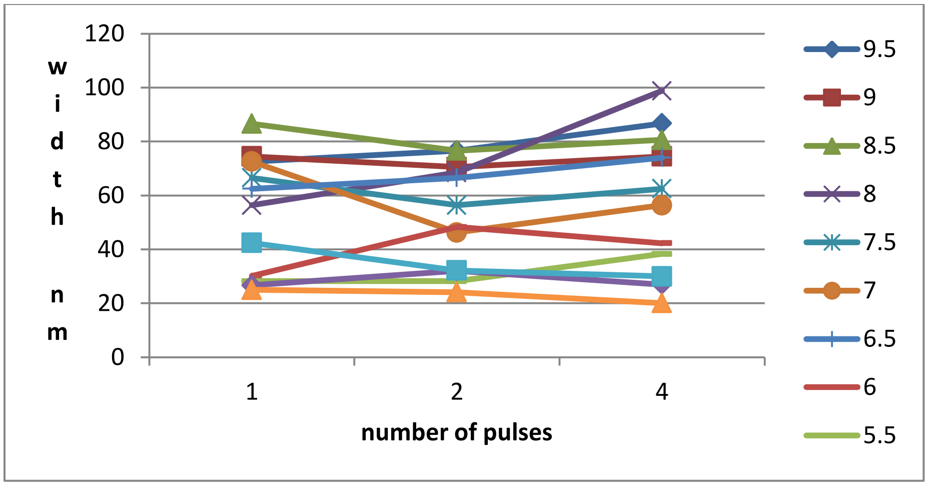

(a)

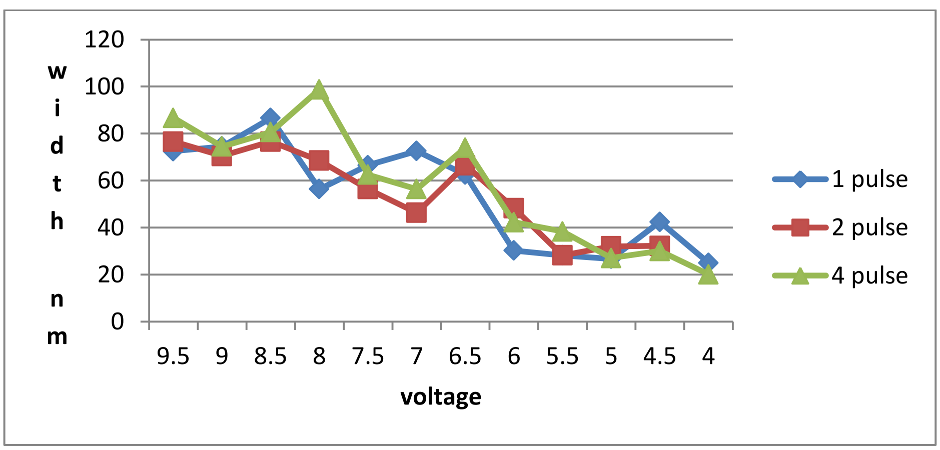

(b)

Figure 18 The width dependence for an 12x3 experiment done with 1,2,4 pulses and voltage decrease from 9.5 to 4 V in steps of 0.5 V on (a) pulse for each voltage, x-axis is number of pulses and (b) voltage for each pulse x-axis is voltage.

The spread of the depth and width of the 7 V, 6 V and 5 V and the 4,8,12 pulses factorial experiment for each of the four trials is shown in Figure 19. The following Table VII depicts the ANOVA using a non-linear model for the 7 V, 6 V, 5 V and 4,8,12 pulses experiment that was repeated four times as described in 4.3. The output variable was depth. Table VIII shows a non-linear model for the for the 7V, 6V, 5 V and 1, 4, 8, pulses experiment. The experiment with 4,8,12 pulses showed an overall greater consistency than 1, 4, 8 pulses because of number of pulses are more spaced out.

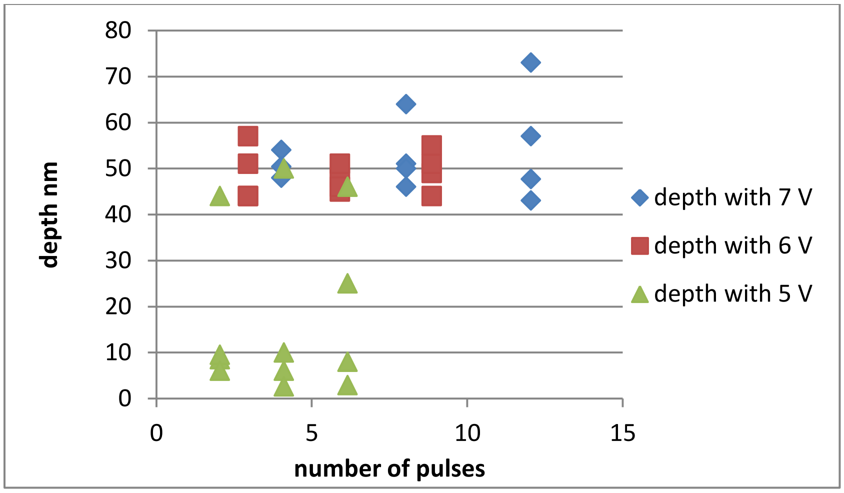

(a)

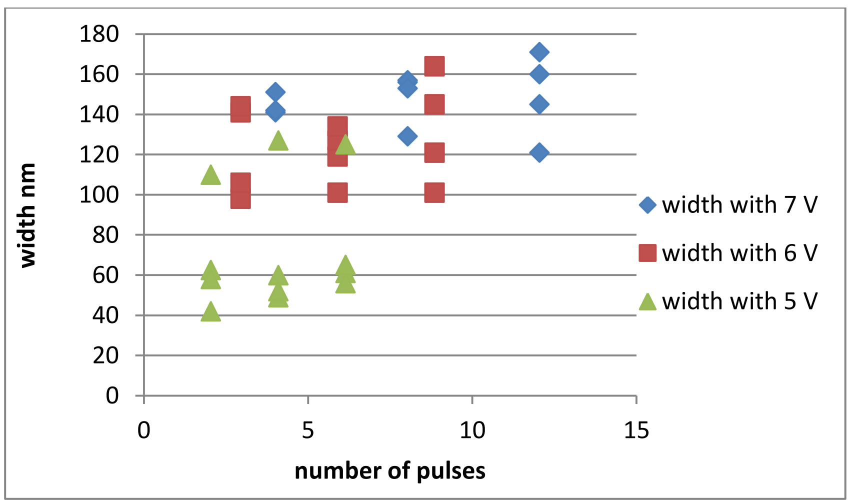

(b)

Figure 19 (a) Depth dependence on pulse for each voltage for all four times repeated and (b) width dependence on pulse for each voltage for all four times repeated for a 3x3 experiment with 7V,6V and 5V and 4,8,12 pulses.

Table VII: A statistical model for the 7V,6V and 5 V and 4,8,12 experiment ,repeated four times, with depth as the output variable ‘Y’. (‘X variable 1’ is ln(PV) and ‘X variable 2’ is ln(P))

3x3 experiment (repeated four times)

Variables: **Voltage ’V’** {7,6,5} , **Number of pulses ‘P’** {1,4,8}

Output: **depth ‘Y’**

Model : **Y = ln(PV) + ln(P)**

SUMMARY OUTPUT

Regression Statistics	
Multiple R	0.747865531
R Square	0.559302853
Adjusted R Square	0.532593935
Standard Error	8.649211531
Observations	36

ANOVA

	df	*SS*	*MS*	*F*	*Significance F*
Regression	2	3133.097	1566.548	20.940678	1.34374E-06
Residual	33	2468.692	74.80886		
Total	35	5601.789			

	Coefficients	*Standard Error*	*t Stat*	*P-value*	*Lower 95%*	*Upper 95%*
Intercept	-105.000854	18.83711	-5.57415	3.386E-06	-143.3252421	-66.6764658
X Variable 1	-66.2427648	10.61382	-6.24118	4.752E-07	-87.8367395	-44.6487902
X Variable 2	67.42611827	10.48202	6.432552	2.716E-07	46.10029393	88.7519426

Table VIII: A statistical model for the 7V,6V and 5 V and 1,4,8 experiment ,repeated four times, with depth as the output variable ‘Y’. (‘X variable 1’ is ln(PV) and ‘X variable 2’ is ln(P)).

3x3 experiment (repeated four times)

Variables: **Voltage ’V’** {7,6,5} , **Number of pulses ‘P’** {4,8,12}

Output: **depth ‘Y’**

Model : **Y = ln(PV) + ln(P)**

SUMMARY OUTPUT

Regression Statistics	
Multiple R	0.7552952
R Square	0.5704709
Adjusted R Square	0.5436253
Standard Error	13.252678
Observations	35

ANOVA

	df	*SS*	*MS*	*F*	*Significance F*
Regression	2	7464.45545	3732.2277	21.25009	1.3424E-06
Residual	32	5620.2714	175.63348		
Total	34	13084.7269			

	Coefficients	*Standard Error*	*t Stat*	*P-value*	*Lower 95%*	*Upper 95%*
Intercept	-153.33679	30.4812037	-5.030536	1.82E-05	-215.42497	-91.24861
X Variable 1	106.40888	16.413593	6.4829731	2.7E-07	72.9754868	139.84228
X Variable 2	-104.50033	17.3812101	-6.012259	1.05E-06	-139.9047	-69.09597

Figure 20 shows the material removal rate which was the volume removed (assuming the holes were modeled by cones) against the duration of nano electro machining or number of pulses. It is a fairly linear increase. Shown below in the Figure 21 is the depth dependence of holes made by the nanowire tip on the voltage (5V, 4.5V and 4V) for various pulses (2, 4 and 8) in a 3x3 factorial experiment. Figure 22 shows the width dependence of the slots made by the standard tip on voltage (7V and 6V) and pulses (4,8) in a 2x2 factorial experiment. In case of the average width of a slot, it is only a rough estimate as measuring the width accurately throughout the length of the slot was quite challenging.

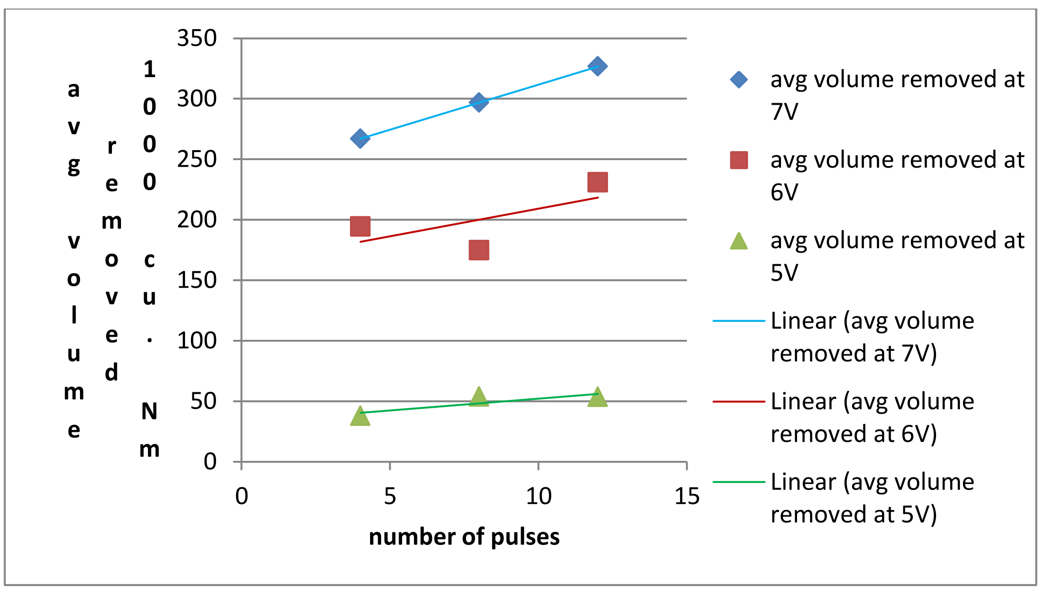

Figure 20 The plot shows the volume of material removal removed (assuming the holes are cones) against the number of pulses or machined time. Y-axis is in 1000 cu. Nm. The x-axis is in seconds. The slope of the curve would give the material removal rate for each voltage.

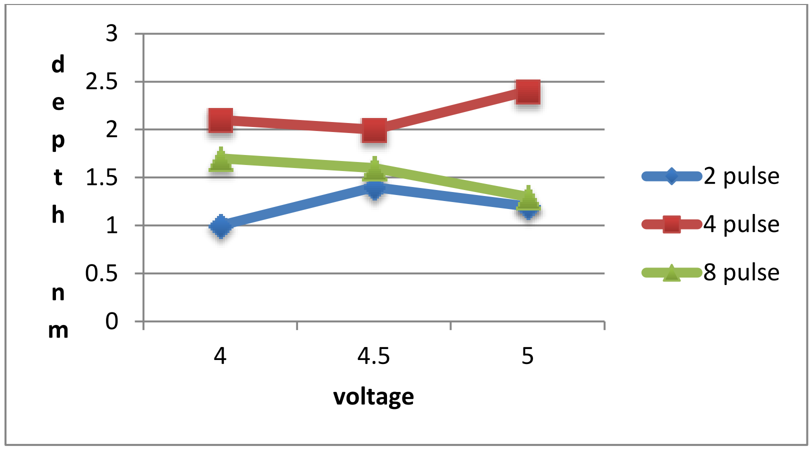

(a)

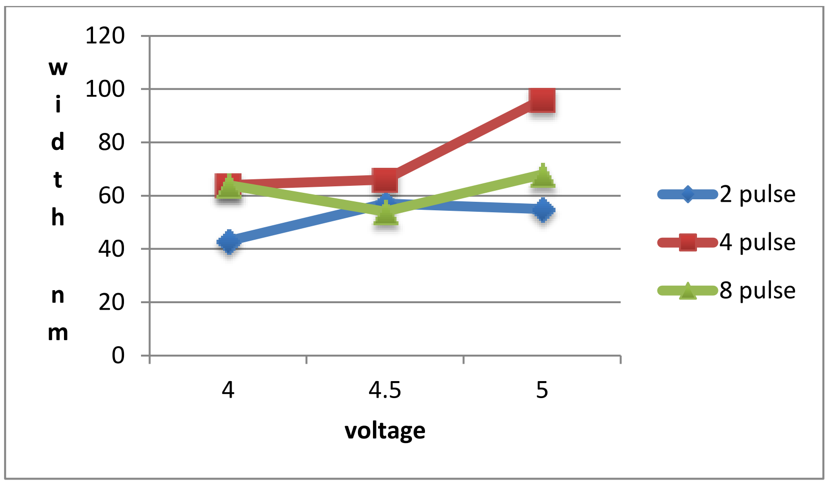

(b)

Figure 21 (a) Depth in nm and (b) width in nm of the holes made by the nanowire in a 3x3 experiment that depends on voltage for each pulse. The decrease in dimension towards the end may attribute to the gradual wearing of the nanowire which stopped working just after this experiment.

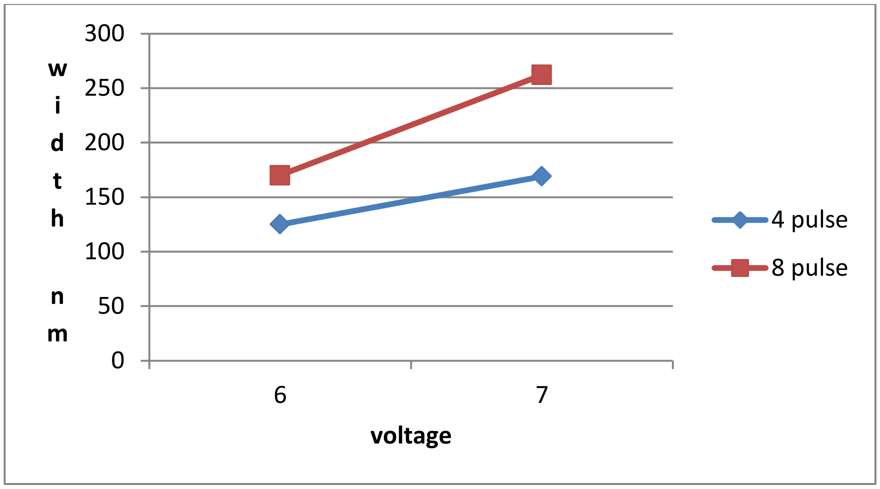

(a)

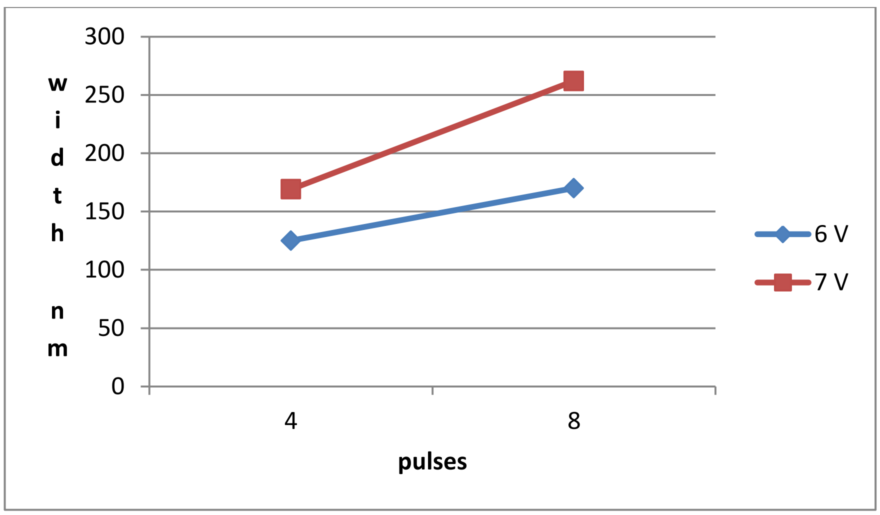

(b)

Figure 22 Width dependence of the slot on the parameters in a 2x2 experiment on (a) pulse for each voltage and (b) voltage for each pulse.

B. Additional Images from the HOPG Experiments

The experiment shown below was done the voltage was varied by 5, 6, 7 V and the number of pulses by 1,4,8. This experiment was performed four times to examine the repeatability as described in Section 4.2. The only difference is the sequence of performing the each experiment, two of which were performed from left to right and the other two from right to left (depicted clearly in Figure 23).

Figure 23 shows the experiment key and corresponding AFM image. The four boxes represent identical factorial experiments. The only difference between four experiments is the difference in the order in which the individual holes are machined within an experiment. Each of the four boxes in Figure 23 (a) corresponds to the each of the colored boxes in the Figure 23(b) which represent each of the four factorial experiments. If the high voltage (7 V) was performed first and then the smaller ones (6V and 5 V), the dimensions (diameter/width and depth) of the holes from lower voltages seem to be much larger than those resulting from the opposite sequence. If the lowest voltage was performed first (5 V) then 6 V and 7 V, the 6 V and 5 V holes seem to be much smaller in dimension than that of the former sequence. The high voltage (7 V in this case) seems to be consistent regardless sequence. This may be some sort of hysteresis. As a general trend, it can be inferred that the consistency is higher when the voltage is higher (above 7 V). The hypotheses behind this phenomenon can be found in Section 4.2.1.

The Figure 24 below shows the 3D image of the above mentioned experiment while Figure 25 shows the inverted 3D image for illustration of the relative depths of the holes.

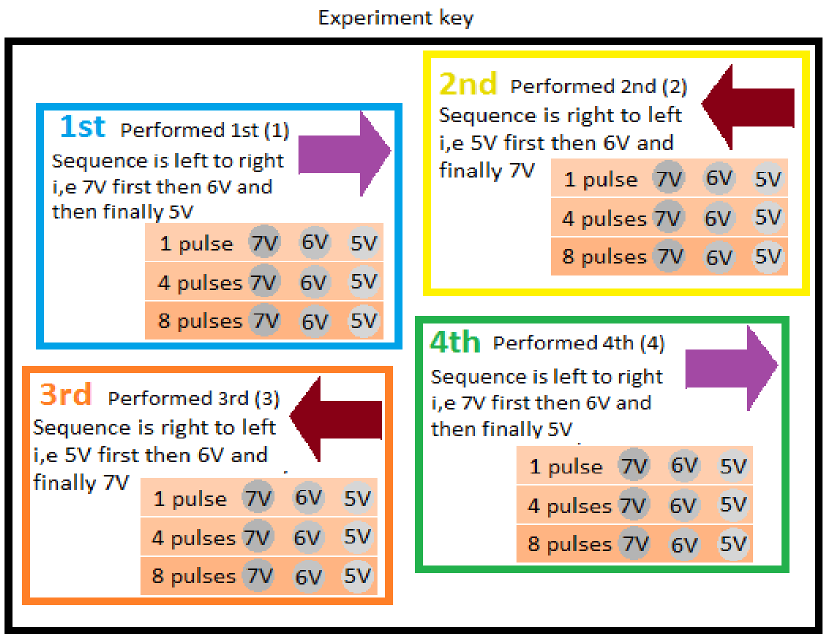

(a)

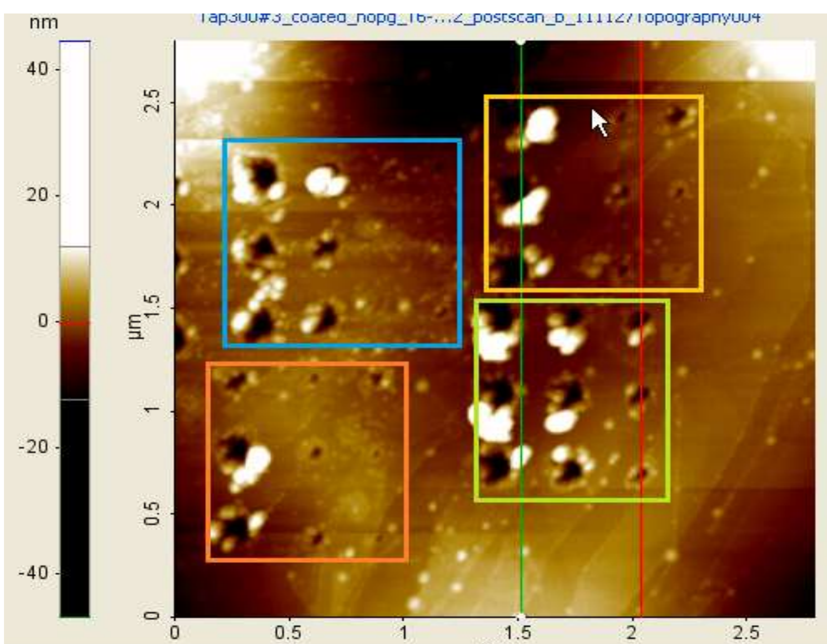

(b)

Figure 23 (a) Key for a factorial experiment (7,V,6V& 5V and 1,4,8 pulses) repeated four times. Each of the four colored boxes in the figure represent the same factorial experiment. The order of nano electro machining within a factorial experiment varies as described in the Figure (a). (b) AFM image of the same experiment. Each of the colored boxes corresponds to the box in Figure 23 (a) which gives the sequencing of machining of each hole within an experiment.

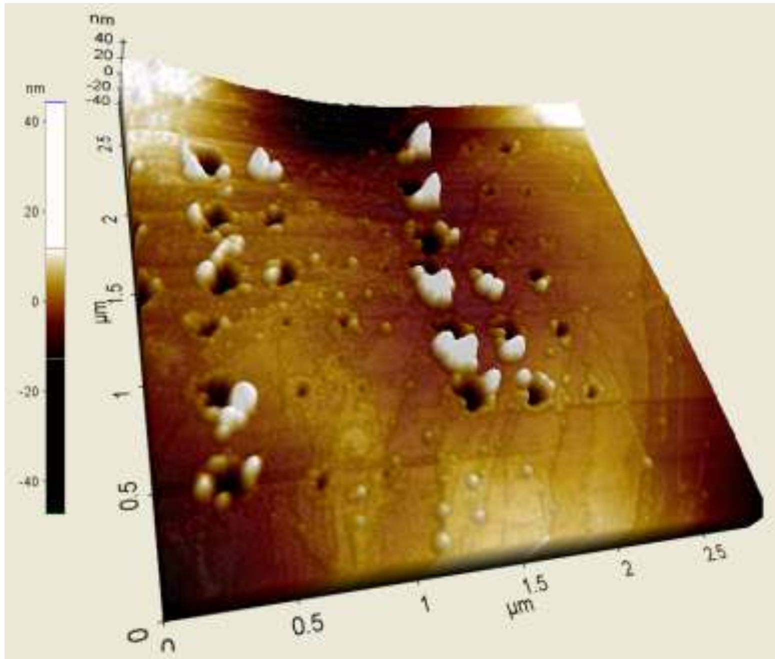

(a)

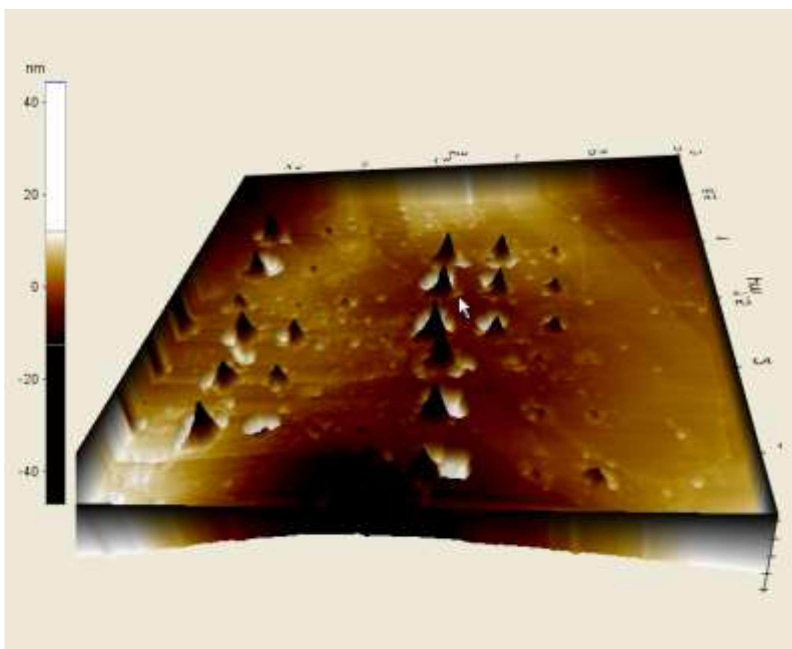

(b)

Figure 24 (a) 3D image of the 3x3 experiment. There are 3x3 four matrices each made by combinations of 5V, 6 V and 7 V and 1,4 and 8 pulses. (b) Inverted image of the 3x3 factorial experiment shown in Figure 24 (a) to show clearly the dimensions of holes.

Figures 25, 26 below show some images from the holes made by the nanowire tip as well as the slots (string of inter-connected holes) made by the standard tip respectively.

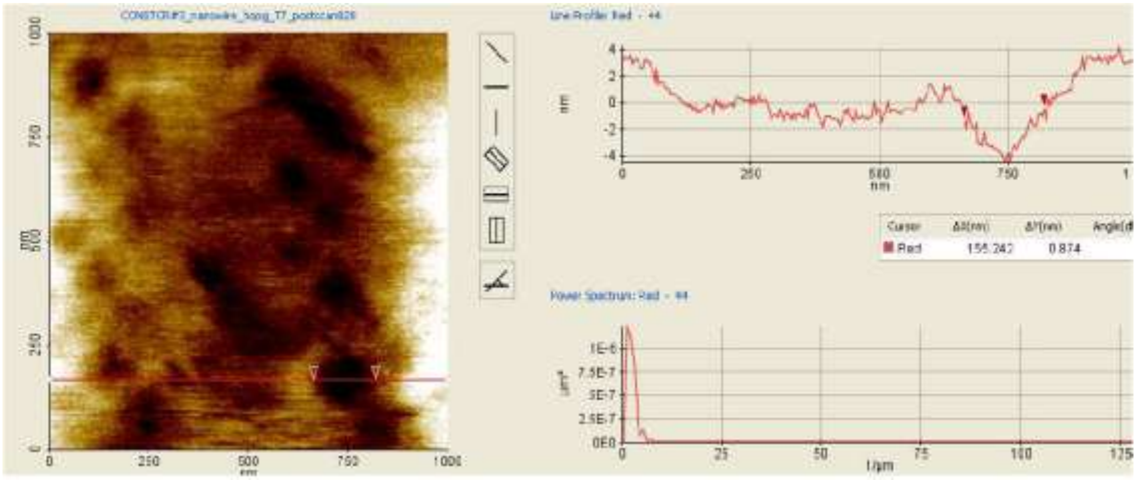

Figure 25 Four holes fabricated using the nanowire with 4 V. There is one hole at each corner of the box. As depicted in Section 4.5 and Section 4.6 the holes made by the nanowire are shallow (slightly higher in depth and much larger in diameter/width) than those made by standard tip.

Figure 27 (a) below shows the experiment performed using the same parameters listed in Section 4.1. The voltage was decreased from 9 V to 4 V in steps of 0.5 V and it was repeated in the next rows with 2 and 4 pulse. The last column was done with 7 V to demonstrate the size decrease was not due to time wear or some other chronological phenomenon. Figure 27 (b) shows the inverted 3D image for illustrative purposes. The sample below lithographically resembles a quantum anti-dot array [4].

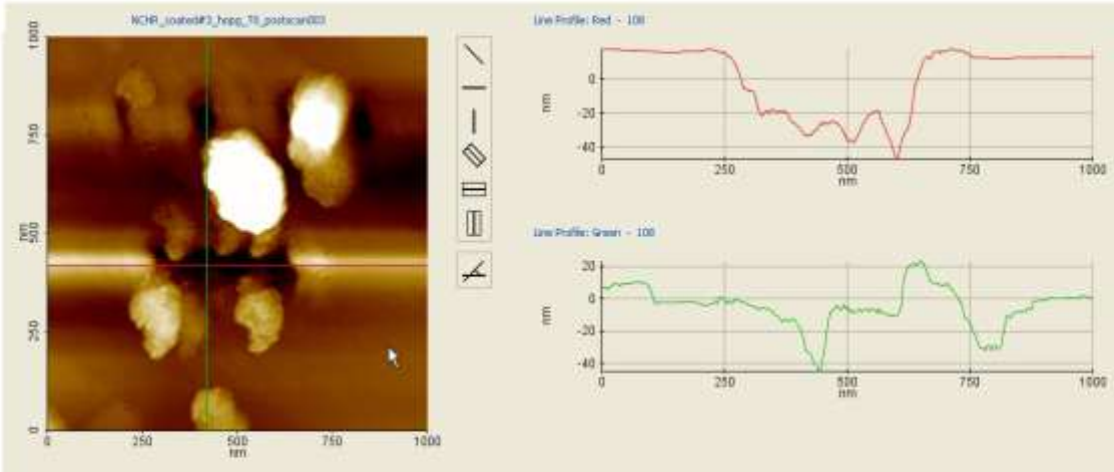

Figure 26 A successfully fabricated slot using 6 V which has the 'best' step-over distance between each hole. The top holes show a failed attempt as the step-over distance between the holes was too large.

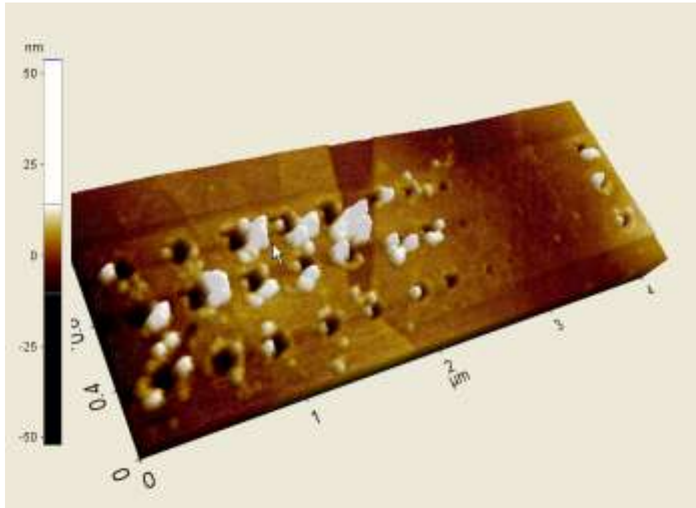

(a)

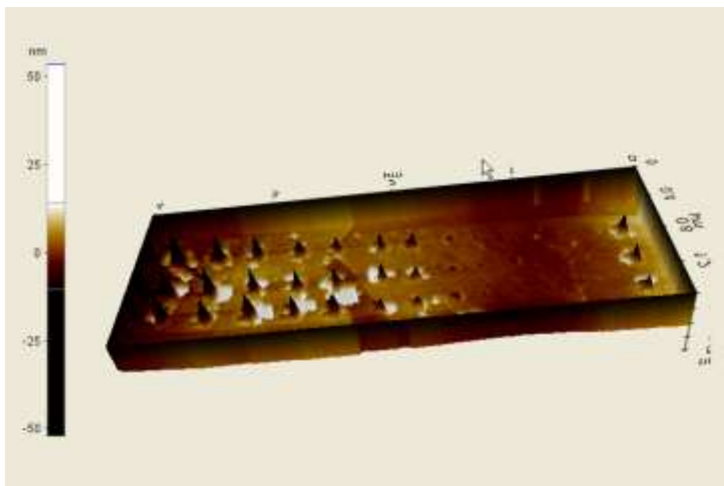

(b)

Figure 27 (a) A 12x3 factorial experiment. Holes are fabricated with varying voltage from 9.5 V to 4 V in steps of 0.5 V and 1, 2 & 4 pulses. This structure resembles a quantum anti-dot array. (b) The inverted image of the same 12x3 experiment shown to illustrate the variation hole depth and diameter with voltage.

C. Images from the Experiments on Aluminum

To test whether nano electro machining is feasible or not, it was first attempted on aluminum. The aluminum sample of around 100 nm in depth was thermally evaporated on a silicon <100> substrate. Because of the rough surface of the sample and its high susceptibility to oxidation, HOPG was selected for further experiments. The Figure 28 shows the first trench made by nano electro machining performed on aluminum. The set point was 5nN and the voltage was negative DC -9.8 V and the tip was moved along a 500 nm line repeatedly for about 6 minutes with a speed of 15 um/second. The voltage eroded the material and made a trench 6 nm deep.

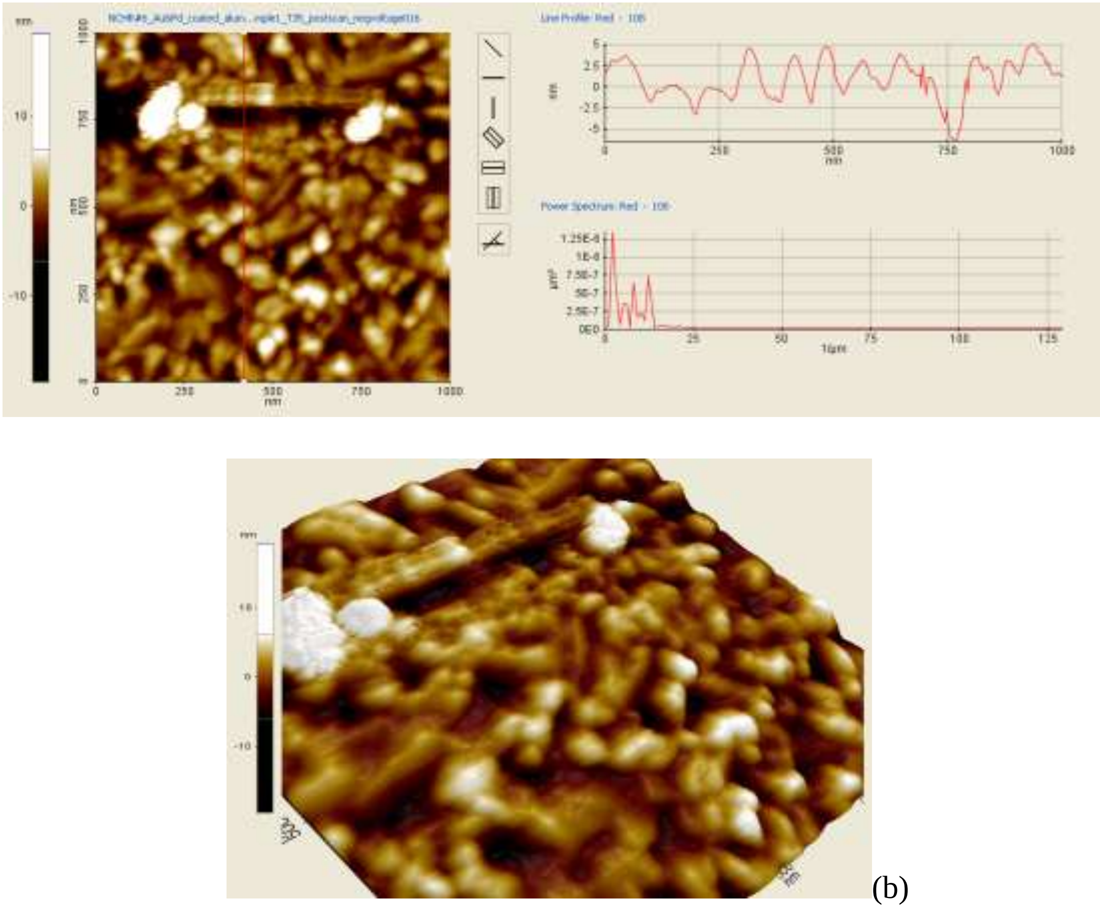

(a)

(b)

Figure 28 (a) A slot fabricated on aluminum by nano electro machining using -9.8 V (b) 3D image of the same trench or slot.

The same experiment was performed several trials later using the same parameters. The slot is not as conspicuous as the very first one as the tip broke down over time, which is depicted in Figure 29.

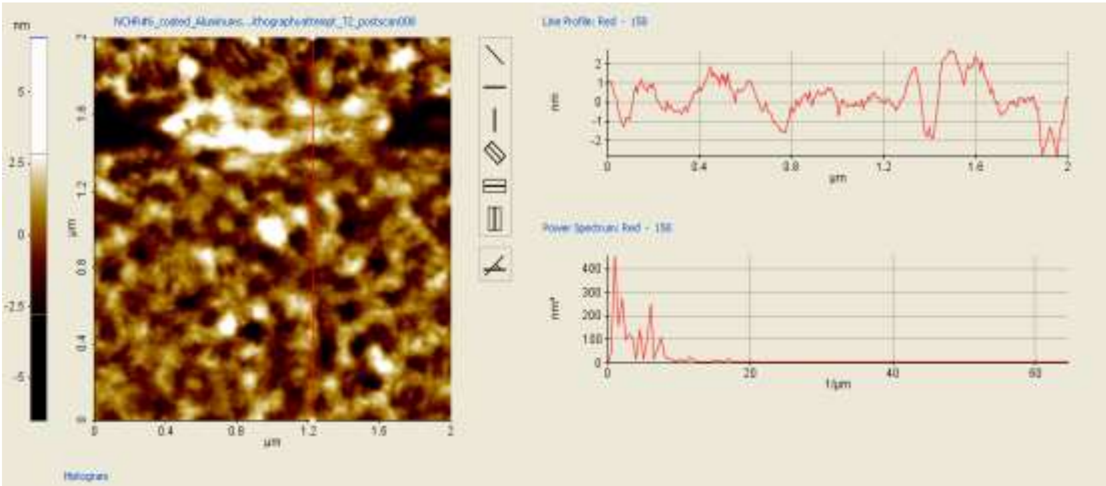

(a)

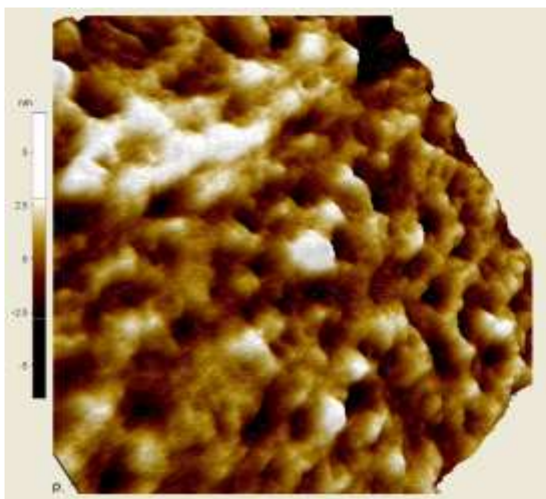

(b)

Figure 29 (a) AFM image of another slot on aluminum made by -9 V. (b) 3D image of the aluminum trench made by -9 V. It is not as conspicuous as the one in Figure 28 because the tip was on the verge of completely wearing out and the roughness of the sample.

D. SEM Images of AFM tips

Nano electro machining performed on HOPG caused wear on the tip. After several experiments of nano electro machining the tip completely breaks down and material removal ceases to occur. Figure 30 shows a typical before and after nano electro machining the HOPG. The melting or evaporation of the tip material may be an integral part of the nano electro machining process in air. A detailed discussion of the alteration of the tip material after nano electro machining can be found in [32]. In order to measure small features such as holes less than 30 nm in diameter or width and less than 5 nm in depth, the profile of the AFM tip must also be of a similar order of dimension.

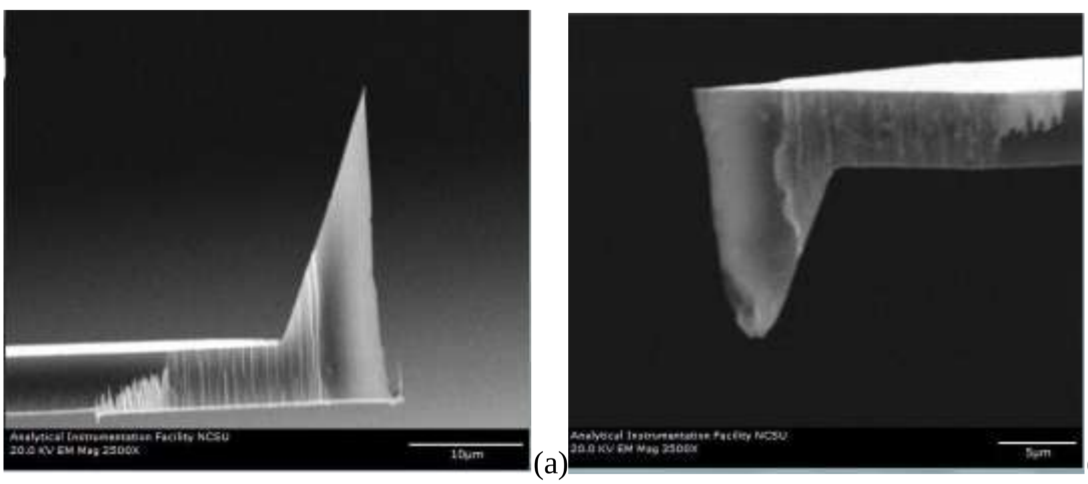

Figure 30 (a) SEM image of a typical brand new silicon tip coated with gold. (tip was pre-coated by the manufacturer; tip was a Ktek tetra-16 Au) (b) And SEM image of the same tip after nano electro machining with around 90 cumulative pulses and with voltages up to 8 V.

Figure 31 below shows the SEM image of a nanowire tip which was used for nano electro machining as described in Section 4.5. The image shows the very tip of the nanowire is curved with a radius of 100 nm. The hemispherical curvature implies that the area which actually comes in contact with the surface should span a few square nanometers. So it must be possible to measure features that are less than 30 nm in dimension as the contact force or set point is always under 5nN. Figure 32 shows an SEM image of the nanowire after some imaging but before nano electro machining. The curvature (radius of which is 100 nm) of the tip ensures that the probe has a very small surface contact area that may facilitate imaging of features that are significantly smaller than 100 nm in dimension. Figure 33 shows the SEM image of a standard tip before attaching the nanowire. The SEM image in Figure 33 represents the typical profile of a standard tip which was used for nano electro machining.

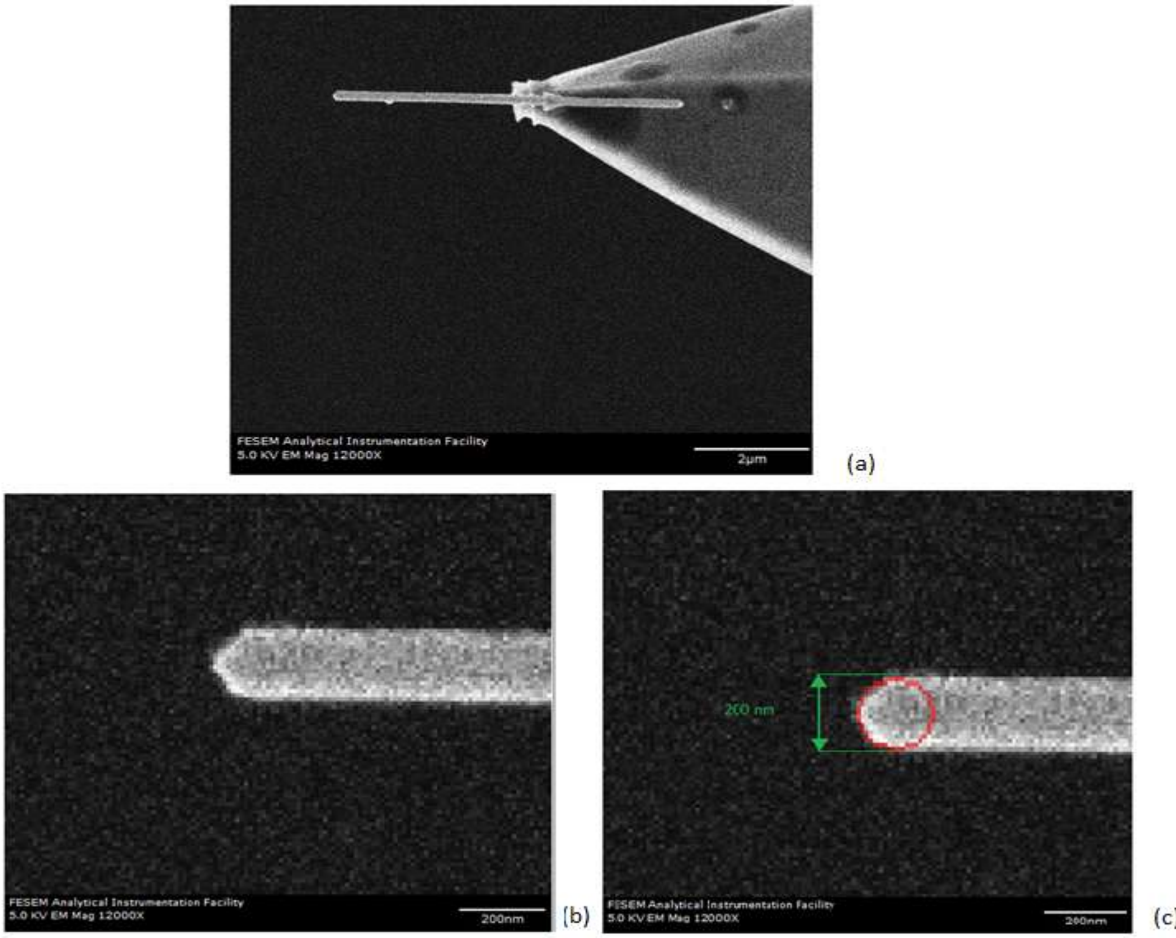

Figure 31 (a) SEM image of a polycrystalline Ag nanowire tip around 3 to 4 um in length attached to a standard tip (b) Magnification of the mentioned tip shows that the very tip is curved (c) The red circle profiles the tip as a hemisphere with 200 nm diameter.

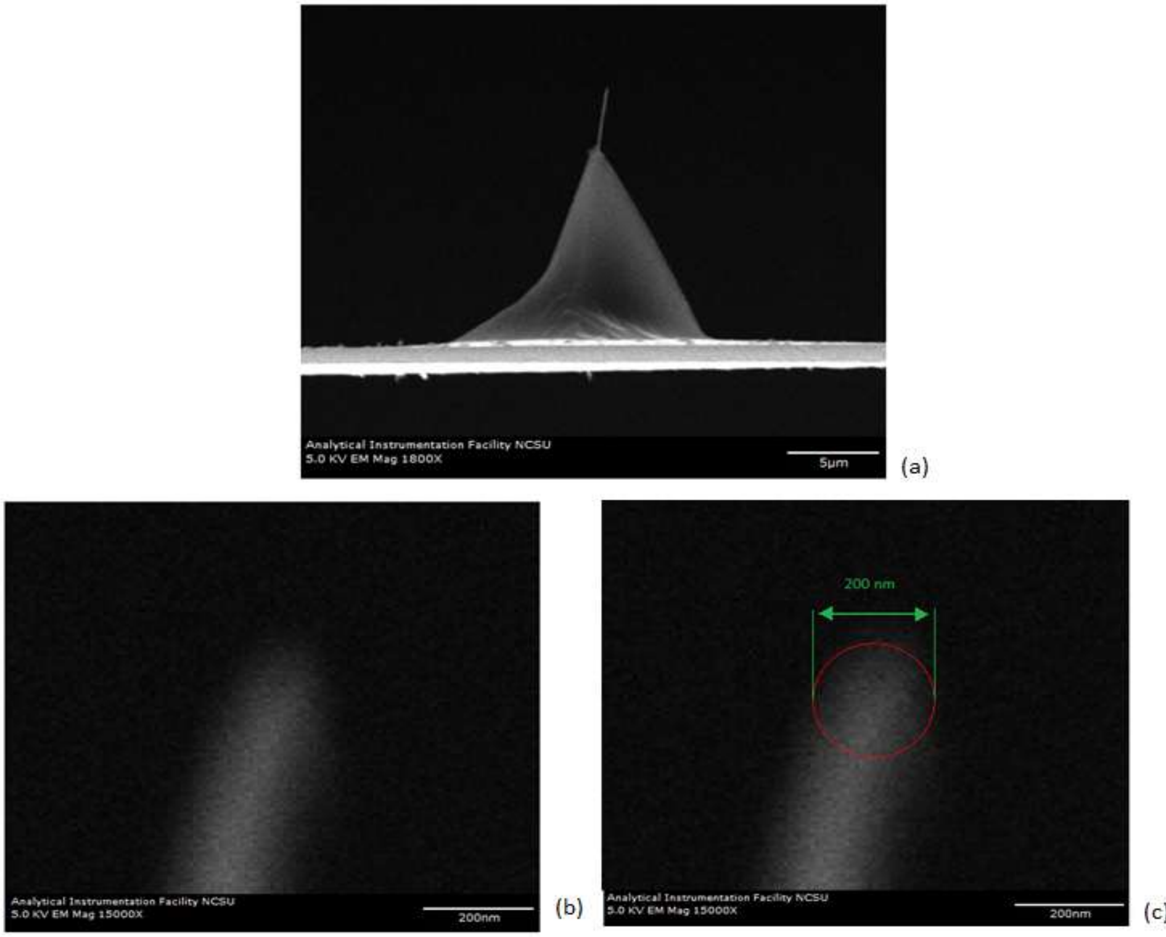

Figure 32 (a) SEM image of a polycrystalline another Ag nanowire tip around 3 to 4 um in length after imaging and just before nano electro machining. Attached to a standard tip (b) Magnification of the mentioned tip shows that the very tip is curved (c) The red circle profiles the tip as a hemisphere with 200 nm diameter.

The bluntness of the tip is due to its prior, extensive use as a mechanical ploughing tool on polymer films in an unrelated project. There are no SEM images of nanowire that depict the profile after nano electro machining like the one in Figure 30, because the nanowire had completely eroded away after completion of the experiment and the SEM image of which closely resembled that in Figure 32.

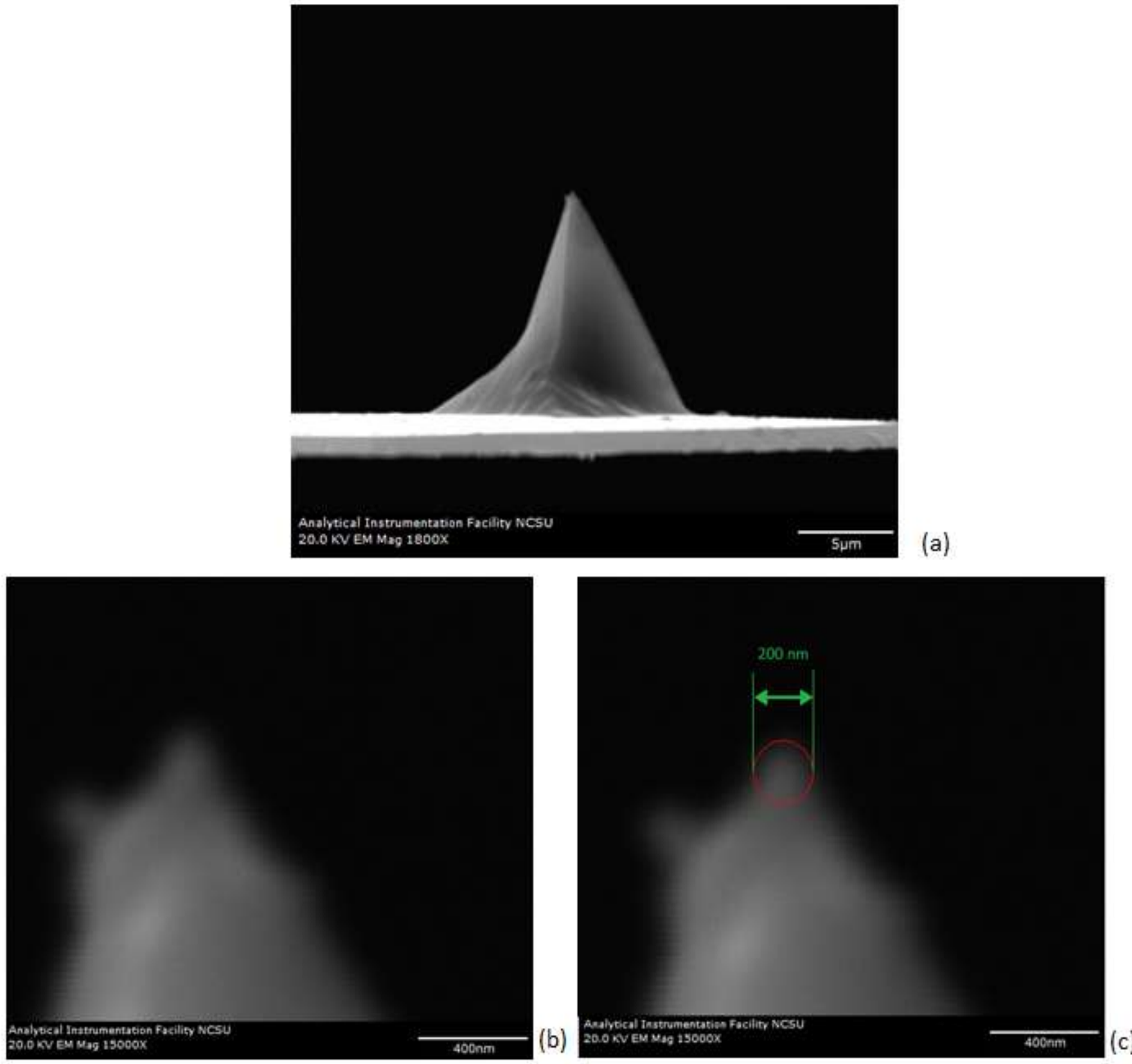

Figure 33 (a) SEM image of a standard tip before attaching a nanowire. This tip represents the profile of a typical standard tip before nano electro machining. (b) Magnification of the mentioned tip shows that the very tip is curved (c) The red circle profiles the tip as a hemisphere with 200 nm diameter. The standard tips that were used for nano electro machining were used previously used extensively as a mechanical ploughing tool on polymer films for an unrelated project.

E. Derivation of the Transmission Coefficient for F.N. Tunneling

The process by which the electron leave the AFM tip is Fowler-Nordheim tunneling as described in Section 4.3. Figure shows the difference in schemes of the Fowler-Nordheim and direct tunneling. The y-axis is energy and the x-axis is distance. A fraction of the electrons jump or tunnel through the potential, applied between the AFM tip and the sample, even though they don't possess enough kinetic energy to do so. Material 1 is the AFM tip and material 2 is the sample in the Figure 34. The F.N. tunneling is associated with a much steeper voltage. Hence the solution is inherently more complex as the electrons leave in the middle of the ramp rather than go directly underneath it as in case of direct tunneling.

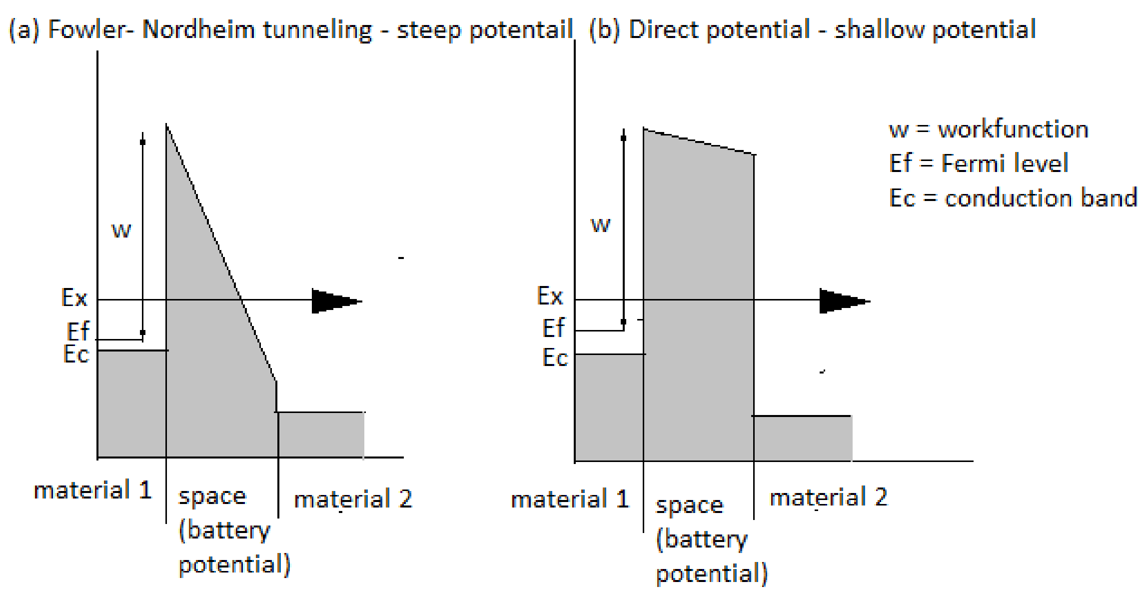

Figure 34 Schematic representation of the two types of tunneling

When a constant electric field is applied between two objects, its profile can be plotted and the potential profile would be a slopped line. When two parallel plates are charged the electric field is a constant. But here the electric field in question is between an AFM tip and the sample. Although the sample is flat, the AFM tip is not flat. Hence the electric field between them is not uniform. Appendix F gives details about the potential distribution and/or electric field distribution around the AFM tip when the AFM tip is treated as a cone. Now we solve the tunneling problem assuming it is between two parallel plates (although it is not the case) and then later modify the result in context of the AFM tips (standard and nanowire) of different aspect ratios.

Let the Schrodinger equation be

$$H \mid \Psi >= E \mid \Psi > \tag{1}$$

Assuming one dimension (1-D)

The H in the above equation refers to the single-particle Hamiltonian of the electron. The Hamiltonian here is the sum of kinetic energy and the potential experienced by the electron from electric field applied to the tip. The Psi refers to the single-particle wavefunction of the electron leaving the tip and E is the energy Eigen value.

Figure 35 shows the potential profile between two charged parallel plate capacitors. Region 0 is material 1 and region l is material 2. The region P is the space in between.

For region P the equation is

$$-(ih^2 \frac{\partial^2}{\partial x^2} - U(x))\Psi(x) = E\Psi(x) => \tag{2}$$

An exact solution to this differential equation does not exist. So we make an approximation for the potential. Figure 36 shows the approximation used. The slope or region ‘P’ in Figure 35 is divided into N segments, each with a piece-wise decrease in potential.

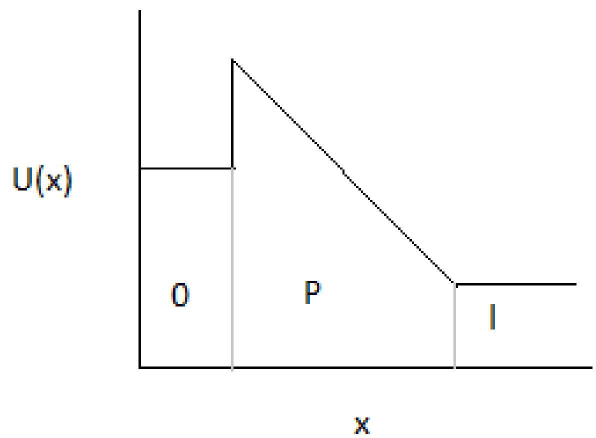

Figure 35 Potential between two materials (region 0 and l) with uniform electric field.

Now let the region P be divided into N Sections each with a piece-wise decrease in the potential. Now an exact solution for this does exist. Each Section ‘i’ is associated with a wavefunction and all the N wavefunctions can now be connected to form continuous wavefunction in the region of the potential. Then the ends of these wavefunctions can be connected with those in region 0 and region l. Figure 37 shows the piece-wise decrease in potential rather than a smooth one. Each step is associated with a separate wavefunction..

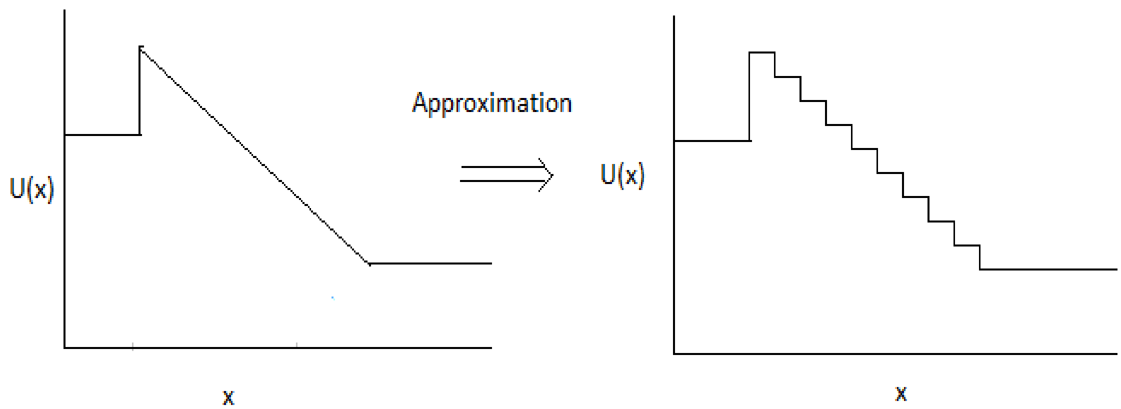

Figure 36 Approximation of the potential from smooth line to piece-wise potential.

Now equation (2) is solved for region P.

Figure 37 shows that potential region P is divided into finite N segments of constant value of potential. Each region 'i' is associated with a wavefunction.

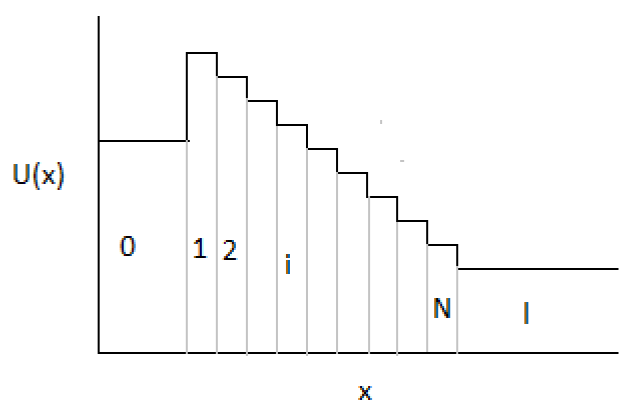

Figure 37 The approximated potential. The stepwise region has N segments.

The schrodinger equation for region 1 is

$$-(ih^2\frac{\partial^2}{\partial x^2} - U_1)\Psi_1 = E\Psi_1 \tag{3}$$

The general solution or wavefunction for the above equation is

$$\Psi_1 = A_1 \exp(k_1 x) + B_1 \exp(-k_1 x) \tag{4}$$

Where

$$k = \sqrt{\frac{2m(U(x) - E)}{h}} \tag{5}$$

For the requirement of continuity for some region i

$$\Psi_i(at\, intersection\, between\, region\, i\, and\, i{+}1) = \Psi_{i+1}(at\, intersection\, between\, region\, i\, and\, i+1) \tag{6}$$

$$\Psi_i'(at\, intersection) = \Psi_{i+1}'(at\, intersection) \tag{7}$$

Thus

$$=> \Psi_1(L/N) = \Psi_2(L/N) \tag{8}$$

Hence for region 1 and 2

$$=> A_1 exp(k_1(L/N)) + B_1 exp(-K_1(L/N)) = A_2 exp(k_2(L/N)) + B_1 exp(-K_2(L/N)) \tag{9}$$

Similarly as

$$\Psi_1'(L/N) = \Psi_2'(L/N) \tag{10}$$

Then for region 1 and 2

$$k_1(A_1 exp(k_1(L/N)) - B_1 exp(-K_1(L/N))) = k_2(A_2 exp(k_2(L/N)) - B_1 exp(-K_2(L/N))) \tag{11}$$

The above equations 9 and 11 can be solved for A2 and B2

$$A_2 = (\frac{k_1 + k_2}{2k_1})exp((L/N)(k_2 - k_1))A_1 + (\frac{k_1 - k_2}{2k_1})exp((L/N)(-k_2 - k_1))B_1 \tag{12}$$

$$B_2 = (\frac{k_1 - k_2}{2k_1})exp((L/N)(k_2 + k_1))A_1 + (\frac{k_1 + k_2}{2k_1})exp((L/N)(-k_2 + k_1))B_1 \tag{13}$$

This can be put in a matrix form

$$\begin{bmatrix} A_2 \\ B_2 \end{bmatrix} = \begin{bmatrix} (\frac{k_1+k_2}{2k_2})exp((L/N)(k_2 - k_1)) & (\frac{k_1-k_2}{2k_2})exp((L/N)(-k_2 - k_1)) \\ (\frac{k_1-k_2}{2k_2})exp((L/N)(k_2 + k_1)) & (\frac{k_1+k_2}{2k_2})exp((L/N)(-k_2 + k_1)) \end{bmatrix} \begin{bmatrix} A_1 \\ B_1 \end{bmatrix} \tag{14}$$

Thus for any sub-regions of P, m and m+1, the matrix can be written as

$$\begin{bmatrix} A_{m+1} \\ B_{m+1} \end{bmatrix} = \begin{bmatrix} (\frac{k_m+k_{m+1}}{2k_{m+1}})exp^{((mL/N)(k_{m+1}-k_m))} & (\frac{k_{m+1}-k_m}{2k_{m+1}})exp^{((mL/N)(-k_{m+1}-k_m))} \\ (\frac{k_{m+1}-k_m}{2k_{m+1}})exp^{((mL/N)(k_{m+1}+k_m))} & (\frac{k_m+k_{m+1}}{2k_{m+1}})exp^{((mL/N)(k_{m+1}-k_m))} \end{bmatrix} \begin{bmatrix} A_m \\ B_m \end{bmatrix} \tag{15}$$

This can be further generalized to any region m>n.

$$\begin{bmatrix} A_m \\ B_m \end{bmatrix} = \begin{bmatrix} (\frac{k_n+k_m}{2k_m})exp^{((L/N)(k_m-\sum_n^{m-1} bk_b))} & (\frac{k_m-k_n}{2k_m})exp^{((L/N)(-\sum_n^m bk_b))} \\ (\frac{k_m-k_n}{2k_m})exp^{((L/N)(\sum_n^m bk_b))} & (\frac{k_n+k_m}{2k_m})exp^{((L/N)(-k_m+\sum_n^{m-1} bk_b))} \end{bmatrix} \begin{bmatrix} A_n \\ B_n \end{bmatrix} \tag{16}$$

So if 'n' in the above equation is taken as 1, and putting in the form of simultaneous equations yields:

$$h^m A^m = 1/2[(f^m + f_*^m)A_1 + (g^m - g_*^m)B_1] \tag{17}$$

$$j^m B^m = 1/2[(f^m - f_*^m)A_1 + (g^m + g_*^m)B_1] \tag{18}$$

Where for equations (17) and (18), the quantities are defined as

$$f^m = e^{L/N(k_{m-1}(m-1) + \ldots + 2K_3 + K_2 + K_1)} \tag{19}$$

$$f_*^m = x_m f^m \tag{20}$$

$$g^m = 1/f^m \tag{21}$$

$$g_*^m = x_m g^m \tag{22}$$

$$x_m = k_1/k_m \tag{23}$$

$$h^m = e^{mk_m(L/N)} \tag{24}$$

$$j^m = 1/h^m \tag{25}$$

N = number of Sections or divisions in region P.

Now coming back to the entire problem i.e. regions 0, P, and l

Let the functions in region 0,1,N,l be

$$\Psi_0 = A_0 e^{ik_0 x} + B_0 e^{-ik_0 x} \tag{26}$$

$$\Psi_1 = A_1 e^{ik_1 x} + B_1 e^{-ik_1 x} \tag{27}$$

$$\Psi_N = A_N e^{ik_N x} + B_N e^{-ik_N x} \tag{28}$$

$$\Psi_l = A_l e^{ik_l x} + B_l e^{-ik_l x} \tag{29}$$

The wavefunction of the first segment 1 and last segment N of the aggregate region P are designated in equations 27 and 28. The wavefunction for the region 0 and l are designated in equations 0 and l. Here we attempt to find the relationship between the various constants A and B for all the four regions.

Let

$$A_0 = 1, B_0 = R, B_l = 0 \tag{30}$$

What equation 30 tells us that no electron gets reflected in region l. If the electron enters that region it does not return. Also all the electrons move towards region P in region 1 and is denoted by Ao. The aim of this is to find the fraction of electrons that propagate away from the region P in region 1 in terms on the electrons that enter the potential P from region 1. These electrons are the fraction that tunnel through the potential P. We use the equations 17 through 25 in equations 26 through 30 to find the value of Al. This is the aim in the next few steps.

And also let

$$r_1 = k_1/k_0, r_2 = k_N/k_l, x_N = k_1/k_N \tag{31}$$

And

$$d_1 = (1 + ir_1),\ d_2(1 - ir_2) \tag{32}$$

Using the same procedure described before for region 0 and region 1 we obtain,

$$1 + R = A_1 + B_1 \tag{33}$$

$$1 - R = ir_1(A_1 - B_1) \tag{34}$$

Combining the above two equations 33 and 34 we obtain

$$2 = A_1 d_1 + B_1 d_2 \tag{35}$$

Following a similar procedure for regions N and l, we find

$$A_N = 1/2[(1+i/r_2)A_l e^{ik_l L} e^{-k_N L}] \tag{36}$$

$$B_N = 1/2[(1-i/r_2)A_l e^{ik_l L} e^{k_N L}] \tag{37}$$

Rewriting equations 17 and 18 for m = N we get

$$A_N = f_1 A_1 + g_1 B_1 \tag{38}$$

$$B_N = f_2 A_1 + g_2 B_1 \tag{39}$$

Where

$$f_1 = (f^N + f_*^N)/2h^N \tag{40}$$

$$f_2 = (f^N - f_*^N)/2j^N \tag{41}$$

$$g_1 = (g^N - g_*^N)/2h^N \tag{42}$$

$$g_2 = (g^N + g_*^N)/2j^N \tag{43}$$

Let

$$A_N = c_1, B_N = c_2 \tag{44}$$

Combining equations 35, 38, 39 and 44 we get

$$2 = \left(\frac{c_1 g_2 - c_2 g_1}{f_1 g_2 - f_2 g_1}\right) d_1 - \left(\frac{c_1 f_2 - c_1 f_1}{f_1 g_2 - f_2 g_1}\right) d_2 \tag{45}$$

Let

$$e^{L/N(Nk_N + (N-2)k_{N-1} + \ldots + K_1)} = e^K \tag{46}$$

$$c_1^* = (1 + i/r_2) \tag{47}$$

$$c_2^* = (1 - i/r_2) \tag{48}$$

And rewriting equations 24 and 25 for m = N we get

$$e^{-k_N L} = j^N \tag{49}$$

$$e^{k_N L} = h^N \tag{50}$$

Using equations 17 through 25 and 35 through 50 it can be found that

$$2 = \frac{A_l(e^{ik_lL})}{4x_N}[-e^{-K}(1-x_N)c_2^*d_1e^{k_NL}+e^{-K}(1+x_N)c_1^*d_1e^{k_NL}-e^K(1-x_N)c_1^*d_2e^{k_NL}+e^K(1+x_N)c_2^*d_2e^{k_NL}] \tag{51}$$

Also let

$$e^{-K}e^{k_NL} = e^{-P} \tag{52}$$

Using equations 47, 48 and 52; 51 reduces to

$$1 = \frac{A_l(e^{ik_lL})}{4x_N}[e^{-P}d_1(x_N+ i/r_2) + e^Pd_2(x_N - i/r_2)] \tag{53}$$

Using equation 32; equation 53 can be reduced to

$$1 = \frac{A_l(e^{ik_lL})}{4x_N}[e^{-P}(x_N(2+i(1/r_1-r_1)))+e^P(x_N(2-i(1/r_1-r_1)))] \tag{54}$$

And then with more manipulation using equation 32, equation 54 yields

$$A_l^2 = T^2 = [\cosh(P)+i/2(1/r_1-r_1)\sinh(P)]^{-2} \tag{55}$$

Defining the transmission coefficient

$$T^2 = [1+\frac{(1+r_1)^2}{4r_1^2}(\sinh^2(P))]^{-1} \tag{56}$$

Let

$$a = \frac{(1+r_1)^2}{4r_1^2} \tag{57}$$

be some constant.

Thus the transmission coefficient squared or the fraction of electrons tunnel is given as

$$T^2 = [1 + a(\sinh^2(P))]^{-1} \tag{58}$$

Using equation 52

$$P \cong [(L/N)\sum_{m}^{N}(m)k_m] - k_N L \tag{59}$$

This can be approximated to

$$P \cong [(L/N)\sum_{m}^{N}(m)k_m] - k_N L \approx \sum_{m}^{N}(m)k_m \approx \int_0^{U^{-1}(\phi-E)} \sqrt{U(x)-E}dx \tag{60}$$

Where

$$k = \sqrt{\frac{2m(U(x)-E)}{h}} \tag{61}$$

Now equation 58 becomes

$$T^2 \approx [1+a(\sinh^2(\int_0^{U^{-1}(\phi-E)} \sqrt{U(x)-E}dx))]^{-1} \tag{62}$$

The transmission coefficient can also be obtained by the WKB approximation as in [36]:

$$TC = exp(\frac{-2}{h}\int_0^{U^{-1}(\phi-E)} \sqrt{2m(U(x)+\phi-E)}dx) \tag{63}$$

The equation obtained by the piece-wise approximation in equation (62) and the one by the WKB (equation 63) method do not differ very much. In fact, if we substitute the formula for sinhP in equation (58) in the limit that exp(P) >> exp(-P) for a positive P then we would obtain the expression very similar to (63). But the piece-wise approximation seems a logical extension to the expression for transmission coefficient obtained in [40], Chapter 3, for the varying potential as in Figure 39.

Having obtained the transmission coefficient (TC), as shown above, we can plug in the different potentials and investigate the transmission coefficient distribution around each type of tip. But before doing this one can guess the result. The transmission coefficient varies as an inverse exponent, so it decreases as the parameter inside the exponent increases. The parameter in the exponent is given by equation (60). This parameter is the area under the curve which is characterized by the difference between the potential around the tip and energy at which the electrons incident the potential. The limits of the integration are between the point of incidence (tip-air interface) and the point at which the potential would equal the incidence energy as shown in Figure 34. The area of the curve is small if the fall of the potential is fast. The gradient of the potential is the electric field. Hence a larger electric field would warrant a smaller area under the curve given by equation (60) which in turn increases the transmission coefficient. Hence by the argument above, transmission coefficient increases as the electric field increases. Consider an AFM tip modeled by a cone (or any geometry that's not spherically symmetric) as shown in Figure 38. If the electric field decreases as the angle theta increases (Figure 38), so must the transmission coefficient. But if the tip were modeled as a sphere the transmission coefficient would be same in all directions. Note that transmission coefficient for Fowler-Nordheim tunneling does not depend on the distance but only on the Electric Field.

Now we attempt to plug in the specific potential distribution for an AFM tip (modeled by a cone) given in Appendix F into equation 63 or 62. As mentioned earlier, the expression for transmission coefficient is for a potential between two parallel plates (constant electric field). By looking at equation 62, it can be noted that some arbitrary potential (between parallel plates or not) can be substituted in equation 62 to obtain the transmission coefficient.

Further, this is a one-dimensional problem. Thus changing the variable to the one in a radial direction in radial coordinate system would give:

$$U(x) \rightarrow U(r) \rightarrow U(r,\theta) = Ar^{\gamma} P_{\gamma}(cos\theta) \tag{64}$$

As mentioned earlier this solution is for a potential between two parallel plates (constant electric field). By looking at equation 62 it may be stated that the exact shape of the potential may be some arbitrary potential (between parallel plates or not) that can be substituted in equation 62 to obtain the transmission coefficient. Here we attempt to substitute the potential in equation (64) described in Appendix F. .

This is a one-dimensional solution with r as variable. Hence the angle in the above equation can be treated as some arbitrary number and not a variable.

Thus equation can be written as

$$\int_0^{U^{-1}(\phi-E))} \sqrt{U(r)+\phi-E}dr = \int_0^{U^{-1}(\phi-E))} \sqrt{(AP_{\gamma}(cos\theta)r^{\gamma}+\phi-E)}dr \tag{65}$$

Now from Figure 38 we can define

$$D = r\sin\theta \tag{66}$$

$$x = D\tan\theta \tag{67}$$

$$r = \frac{D}{\sin(\arctan x/D)} \tag{68}$$

$$\theta = \arctan x/D \tag{69}$$

Now using the equations we can find the transmission coefficient in terms of the horizontal distance x (refer Figure 38 for clarity). This simple calculation is not shown to reduce the length of the document. The value for gamma in equation 64 depends directly on the characteristic cone angle of the cone. For the standard tip the characteristic angle is assumed to around 50 degrees and for the nanowire it is assumed to be <2 degrees as explained in Section 4.6. The values for gamma for these characteristic angles can be obtained from Appendix F. Thus we have two different integrals in equation 64 for standard tip and nanowire. These can be substituted in equation 62 to obtain two different transmission coefficient distributions for nanowire and standard tip. And these distributions are the functions of the horizontal distance x. When equation 62 is plotted against x for each case for some arbitrary constant A we obtain the Figure 14 or Figure 15 in Section 4.6.

F. Distribution of Electric Field and Potential for Standard and Nanowire Tips

As described in Section 4.6, the standard tip and nanowire can be treated as cones with different characteristic angles. Let the characteristic angle for standard tip and the nanowire be 50 degrees and 2 degrees respectively. Figure 38 shows this scheme.

When a potential is applied between the AFM tip and sample, electrons flow between them as described in Section 4.6 and Appendix E. When a constant potential is applied between the AFM tip and the sample, the tip becomes charged (because in this case, negative pulses are sent to the AFM tip). Although the applied battery potential remains constant, its distribution around the AFM tip may vary because the AFM tip is not flat surface. A non-flat surface does not produce a uniform electric field.

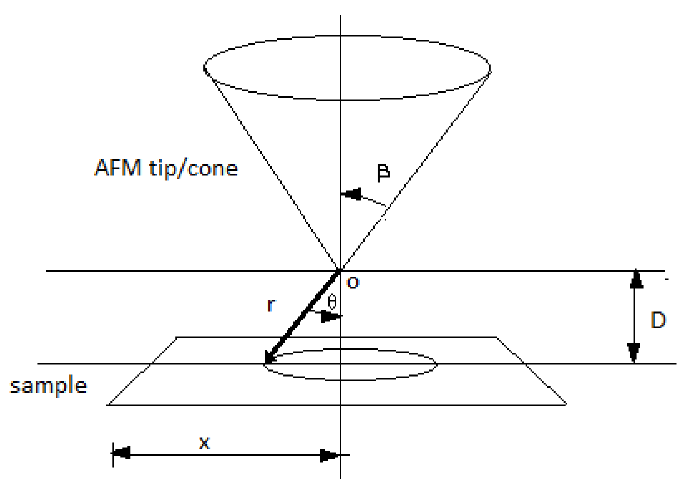

Figure 38 The representation of an AFM tip by a cone.

The electric potential distribution is also non-uniform because the electric potential is the derivative of the electric field [39]. The potential may be stronger in some regions than the others. This might because the surface charge distribution on the tip is not uniform. The surface charge distribution accumulates around a sharp edge [38]. From Jackson [39], the expression for the electric field, potential and surface charge distribution can be obtained for a cone and is given in equations 1, 2, 3.

$$V = \sum_{v_k} (P_{v_k}(cos(\theta)(A_{v_k} r^{v_k} + B_{v_k} r^{-v_k-1}) \tag{70}$$

One of the boundary conditions for (70) is given by (71)

$$(P_{v_k}(cos(\beta)) = 0 \tag{71}$$

Because of the absence of other boundary conditions such as surface potentials, a general solution is taken from [37] for region just outside the tip in (equation 72). More boundary conditions are required to calculate fields at large distances. Only the region near tip is required in this case as tunneling does not occur at large distances.

$$V \quad \alpha \quad r^{v_0} P_{v_k}(cos(\theta)) \tag{72}$$

The gamma in the equations 70 through 73 is directly related to the characteristic angle of the cone. When the angle is 50 degrees gamma is approximately 0.333 and when the characteristic angle is 2 degrees, gamma is around 0.2 [37]. Thus we have two different expressions of the above quantities for the standard tip and the nanowire tip. The U(x) described in equation 62 of Appendix E points to equation 1 here. Thus by equation 62 we have two expressions for transmission coefficient for the standard and the nanowire tip which can be plotted as in Figure 15 in Section 4.6.